Physical and biological effects on the carbonate system during summer in the northern Argentine Continental Shelf (southwestern Atlantic)

Carla F. Berghoff [a*], Denis Pierrot [b], Lucia Epherra [a,c], Ricardo I. Silva [a], Valeria Segura [a], Rubén M. Negri [a], M. Constanza Hozbor [a], Mario O. Carignan [a], Leticia Barbero [b,d], Vivian A. Lutz [a,c]

[a] Instituto Nacional de Investigación y Desarrollo Pesquero (INIDEP), Paseo Victoria Ocampo N°1, B7602HSA, Mar del Plata, Argentina.

[b] Atlantic Oceanographic and Meteorological Laboratory, National Oceanic and Atmospheric Administration (AOML/NOAA), Miami, United States. 4301 Rickenbacker Causeway, Miami, FL, 33149, United States.

[c] Consejo Nacional de Investigaciones Científicas y Técnicas (CONICET), Argentina.

[d] Cooperative Institute for Marine and Atmospheric Studies (CIMAS), Rosenstiel School for Marine and Atmospheric Science, University of Miami, 4600 Rickenbacker Causeway, Miami, FL, 33149, United States.

[*]**Corresponding author**:

Address: Instituto Nacional de Investigación y Desarrollo Pesquero (INIDEP), Paseo Victoria Ocampo N°1, B7602HSA, Mar del Plata, Argentina.
E-mail address: cberghoff@inidep.edu.ar
Phone number: + 54 223 4209100 (ext. 1450)

Running headline: Carbonate system in the Northern Argentine Shelf

For publication in

Journal of Marine Systems

ABSTRACT

The Argentine shelf and its shelf-break (Southwestern Atlantic Ocean) are known for their high biological productivity, and as an important CO_2 sink region. However, many aspects of the carbonate system dynamics in the area, especially those related to the biological activity, deserve further study. Here we investigated the mechanisms affecting the carbonate system distributions, using *in situ* physical, chemical and biological observations collected along a section (COSTAL-AR) on the Northern Argentine Continental Shelf during two summer cruises in 2019. Our main goal was to evaluate the role of the microbial communities on the modulation of the carbonate system in the area. For that, we characterized (i) the distribution of the thermohaline properties, chlorophyll a, dissolved oxygen, carbonate system (pH, total alkalinity, dissolved inorganic carbon and high resolution underway CO_2 fugacity, fCO_2), dissolved inorganic nutrients, and (ii) the microbial communities (bacterioplankton, phytoplankton, and protozooplankton). Our results show that the COSTAL-AR section was likely an important CO_2 sink and presented high seawater fCO_2 spatial variability in both middle (272-430 µatm) or early (211-365 µatm) summer conditions. Phytoplankton played a key role in modulating the CO_2 uptake and carbonate system spatial variability during summer, especially in the middle and outer shelf. The main contribution to CO_2 fixation was given by small cells, since the microbial community was dominated by autotrophic picoplankton (<2 µm; e.g. *Synechococcus* sp. and coccal picophytoeukaryotes). Moreover, the influence of the Shelf-break front in ruling both the seawater fCO_2 distribution and biological processes was evident. These findings provide new insights on the connection between the biology and the carbonate system in this sparsely sampled area of the southwestern Atlantic Ocean.

Keywords: carbonate system, biological activity, chlorophyll a, phytoplankton, bacterioplankton, Argentine Continental Shelf.

1. INTRODUCTION

The ocean's absorption of anthropogenic carbon dioxide (CO_2) plays a key role in moderating climate change; however, this capture affects the chemistry of the ocean carbonate system, a consequence of which is a phenomenon called ocean acidification (Orr et al., 2005; Doney et al., 2009). Ocean acidification shifts the carbonate system by increasing the surface ocean partial pressure of CO_2 (pCO_2), dissolved inorganic carbon (DIC) and hydrogen ions concentrations with the consequent decrease in pH and in carbonate ion concentrations. These changes in the carbonate system speciation also reduce calcium carbonate saturation state and the CO_2 buffering capacity (Riebesell et al., 2009). Models have estimated a surface global ocean pH decrease of ~0.11 units since 1750 (Gattuso et al., 2015), which is consistent with observations registered at time-series sites and along hydrographic sections (e.g., Bates et al., 2014; Takahashi et al. 2014; Lauvset et al., 2015; Fontela et al., 2021; Iida et al., 2021). Therefore, reinforcing the importance of improving the estimations of the carbonate system (pCO_2 in sea and air, sea-air CO_2 fluxes and pH) and its spatiotemporal variability.

The global surface ocean is presently a net sink for atmospheric CO_2, absorbing an estimated 2.8 ± 0.4 Pg C yr^{-1} for the 2011-2020 period (Friedlingstein et al., 2022). The sea-air CO_2 exchange displays a heterogeneous distribution across both space and time, which is controlled by the interaction of the physical and biological carbon pumps (Volk and Hoffert, 1985). Continental shelves present higher spatiotemporal CO_2 variability than the open ocean due to the complex physical and biogeochemical dynamics (Bauer et al., 2013; Gruber, 2015; Laruelle et al., 2014, 2017; Roobaert et al., 2019; Cao et al., 2020). Changes in carbon fixation via primary production, degradation and export of organic carbon are major processes driving the CO_2 variations in continental shelves, though each region may behave differently depending on the seasonality of the upper ocean and the circulation of water masses (Borges et al., 2005; Chen et al., 2013; Gruber, 2015). Phytoplankton has a strong direct impact on sea surface pCO_2 distribution, controlling the uptake of CO_2 especially in the middle and outer shelves; whereas respiration may dominate in the coastal and inner shelf regimes, in this way acting as a source of CO_2 (Chen and Borges, 2009). Although on a global scale continental shelves are net autotrophic, and a sink for atmospheric CO_2 (0.19 ± 0.05 Pg C yr^{-1} for the 1990-2011 period, Laruelle et al., 2014; 0.15 ± 0.01 Pg C yr^{-1} for the 1985-2019 period, Chau et al., 2022), there is still an uncertainty on the regional sea-air CO_2 fluxes estimates, associated to the poor knowledge of processes that control the CO_2 variability in

each case. Overall, the Southwestern Atlantic Ocean acts as a sink of atmospheric CO_2 south of 30˚S (0.3-0.6 Pg C yr^{-1} according to Takahashi et al., 2002), and is close to equilibrium with the atmospheric CO_2 to the north. In recent years the role of the Southwestern Atlantic Ocean in the CO_2 uptake has received special attention (Bianchi et al., 2005, 2009; Ito et al., 2005, 2016; Padin et al., 2010; Arruda et al., 2015; Lencina-Avila et al., 2016; Kahl et al., 2017; Orselli et al., 2018; de Carvalho-Borges et al., 2018; Carvalho et al., 2021; Fontela et al., 2021; Liutti et al., 2021; de Oliveira Carvalho et al., 2022), though this region still remains under-sampled. Specifically regarding the shelf areas in the Southwestern Atlantic, as result of the relevance of biological processes (mainly primary production) on the sea-air CO_2 exchange a contrasting behavior of CO_2 sink-source to the north (source) and south (sink) of 35°S was found, acting as two distinct biogeochemical regions (de Oliveira Carvalho et al., 2022).

The Argentine continental shelf (ca. 34°S-55°S) and its shelf-break has high chlorophyll a concentrations according to satellite images (Romero et al., 2006; Dogliotti et al., 2014; Marrari et al., 2017), and is a highly productive area of the world ocean (spring field estimates of primary production are as high as 5477 mg C m^{-2} d^{-1}; Lutz et al., 2010; Segura et al., 2013), sustaining commercially important populations of fish and invertebrates (Sánchez and Bezzi, 2004). Along with the recognition of its high biological productivity, previous studies denoted that the Argentine shelf and slope waters are an important CO_2 sink area (0.02 Pg C yr^{-1} for the 38°S-55°S latitude band; Kahl et al., 2017) that exhibits a highly seasonal CO_2 dynamic, with marked differences north and south of 47°S, and strong gradients in the frontal regions (Bianchi al., 2005, 2009; Schloss et al., 2007; Padin et al., 2010; Kahl et al., 2017; Orselli et al., 2018). According to these studies, the biological pump dominates the sea-air exchange of CO_2, though the role of plankton communities affecting the carbonate system variability is still poorly understood (see Schloss et al., 2007; Carvalho et al., 2021; de Oliveira Carvalho et al., 2022).

This study is focused on the Northern Argentine Continental Shelf (34˚S-43˚S), an area with a complex hydrography (see section 2.1) that supports coastal and offshore multispecific fisheries for Argentina and Uruguay (e.g. the Argentine anchovy *Engraulis anchoita* and the Argentine hake *Merluccius hubbsi*); being a spawning and breeding area for several species of fish (Auad and Martos, 2012; Marrari et al., 2013; Temperoni et al., 2021). Despite several studies in the area have emphasized the strong influence of both biology and the

thermohaline regime in modulating the CO_2 distribution (Kahl et al., 2017; Kahl, 2018; Orselli et al., 2018; de Oliveira Carvalho et al., 2022), many aspects of its dynamics remain undetermined. The complexity of this area highlights the importance of conducting small-scale observations to reduce the uncertainty of the ocean CO_2 uptake when considering its contribution on the carbon budget at a large scale.

Located in the Northern Argentine Continental Shelf, the "COSTAL" time-series sections from the coast (in Spanish COSta) to the shelf-break (in Spanish TALud) are aimed to assess changes in the marine environment and plankton communities under a global change scenario (Lutz and Carreto, 1991; Carreto et al.,1995; Negri et al., 2016; Cepeda et al., 2020). Within this framework, our main goal was to evaluate the role of the microbial communities on the modulation of the carbonate system along the COSTAL-AR section ("AR" identifies the section starting from Mar del Plata, Argentina, figure 1) during two summer cruises in 2019. For this we characterized: (1) the distribution of the physicochemical properties temperature, salinity, chlorophyll a (Chla), dissolved oxygen (DO), carbonate system (pH, total alkalinity (TA), DIC and CO_2 fugacities) and dissolved inorganic nutrients, and (2) the microbial communities (bacterioplankton, phytoplankton, and protozooplankton). At a broader scale, these new observations complement previous studies and offer an interesting benchmark case to test coupled physical/biological models in this complex dynamical region where field data is still limited.

2. METHODS

2.1. Study area

The Northern Argentine Continental Shelf is an area dominated by Subantarctic Shelf Waters (temperature <21 °C, salinity 33.5-34.2; Möller et al., 2008) advected from the northern Patagonian shelf (figure 1, left). This area is influenced by: (1) the continental discharge of La Plata River, the second largest river in South America; (2) the Shelf-break front, as a result from the meeting of Subantarctic Shelf Waters with the cooler and more saline slope waters derived from advected waters of subantarctic origin within the Malvinas Current (temperature <11°C, salinity >33.9; Martos and Piccolo, 1988; Piola et al., 2010); and (3) by its proximity to the Brazil-Malvinas Confluence (Piola and Matano, 2001). During the spring-summer period, La Plata River plume waters, driven by seasonally reversing winds, flow to the south and east (Guerrero et al., 2014) and there is an invasion of high salinity waters

from El Rincón and Subantarctic Shelf Waters into the coastal areas (Lucas et al., 2005). A moderate thermal front called Mid-shelf front is established between the 30 and 80 m isobaths along the shelf of the Buenos Aires province (38°S-42°S), separating vertically homogeneous coastal waters from seasonally stratified mid-shelf waters (Carreto et al., 1995; Martos and Piccolo, 1988; Lucas et al., 2005; Romero et al., 2006). The Shelf-break front is a permanent thermohaline feature, and its position varies seasonally around 38-39˚S, moving offshore during summer and onshore during spring and autumn, with high biological productivity (Lutz and Carreto, 1991; Carreto et al., 1995; Lutz et al., 2010, Segura et al., 2013; Derisio et al., 2018). Off the shelf and south of about 38°S, the Brazil-Malvinas Confluence, the encounter of the warm southward-flowing Brazil Current and the cold northward-flowing Malvinas Current, promotes energetic exchanges between shelf and deep ocean waters (Saraceno and Provost, 2012).

2.2. Data acquisition strategy

Two multidisciplinary environmental cruises (VA-01/19 and VA-12/19) were carried out aboard the *R/V Víctor Angelescu* during two summer periods in 2019, almost a year apart (24-27 January 2019 and 11-13 December 2019). Samples were collected along the COSTAL-AR section on six stations (figure 1) distributed across the Northern Argentine Continental Shelf in a southeasterly direction, from the coastal sector of Mar del Plata, Argentina (38°13´S-57°17´W) through the shelf-break (39°23´S-55°13´W). The geographical position and total depth of the COSTAL-AR stations, as well as date-time of sampling during the VA-01/19 and VA-12/19 cruises are detailed in table A1. Profiles of temperature and salinity were recorded at each station with a Seabird SBE 911 plus CTD-rosette equipped with dual temperature and conductivity sensors, a SBE 43 dissolved oxygen sensor, a Seapoint fluorometer and 12 10-L Niskin bottles. Discrete seawater samples were collected at 5 m and at two or three other selected depths, for the analysis of DO, pH, TA, dissolved inorganic nutrients, Chla and the microbial community. Discrete salinity samples were used to calibrate the conductivity sensors and were analyzed with an Autosal Guidline 8400B salinometer using IAPSO standard seawater. Physical data were processed using standard Seabird Data Processing software routines. The accuracy of the temperature and salinity sensor measurements were ± 0.001 °C and ± 0.002, respectively for both cruises (Baldoni, 2021).

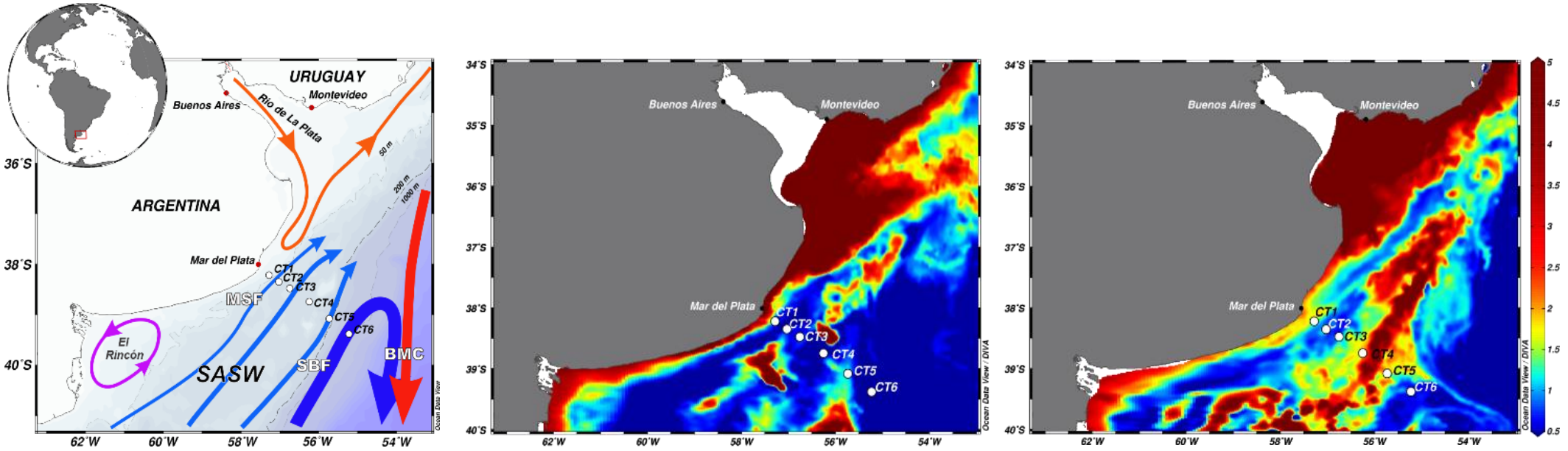

Figure 1. Maps of the study area in the Northern Argentinean Continental Shelf. Left: location of the CTD stations along the COSTAL-AR section (white circles) with schematic surface circulation of Subantarctic Shelf Waters (SASW, blue arrows), Malvinas Current (blue thick arrow), Brazil Current (red thick arrow), La Plata river (orange arrow), El Rincón waters (purple arrow), the Mid-shelf front (MSF), the Shelf-break front (SBF) and Brazil-Malvinas Confluence (BMC); adapted from Matano et al. (2010). Center and right: location of the CTD stations along the COSTAL-AR section superimposed to a MODIS-Aqua chlorophyll a concentration (mg m^{-3}) composite image (4 km resolution) for the time of the cruises. Center: VA-01/19 cruise (24-27 January 2019); right: VA-12/19 cruise (11-13 December 2019).

2.3. Chemical and biological analyses

DO samples were collected in "BOD" borosilicate flasks and analyzed onboard following the Winkler method (Strickland and Parsons, 1972). Precision of DO measurements, through pooled standard deviation of replicate samples collected from the same Niskin bottle, was ± 0.5 µmol kg^{-1}. The SBE43-DO sensor data were post-calibrated with these Winkler samples following the recommendations by Bittig et al. (2018).

Dissolved inorganic nutrients samples were collected in 5 ml-cryovials, preserved in liquid nitrogen on board and then in an ultra-freezer (-86°C) until analysis back on land. Simultaneous determinations of nitrate, nitrite, phosphate and silicate were performed using a SKALAR segmented flow auto-analyzer, following Aoyama et al. (2013) and Becker et al. (2019). Measurement consistency was assessed with Certified Reference Material (CRM; Lot. CG, 2018, Kanso Co., Osaka). Precision of dissolved inorganic nutrients measurements, through pooled standard deviation of replicate samples collected from the same Niskin bottle, were ± 0.10 µmol kg^{-1}, ±0.02 µmol kg^{-1}, ±0.04 µmol kg^{-1} and ±0.20 µmol kg^{-1} for nitrate, nitrite, phosphate and silicate, respectively.

pH samples were collected directly into 10 cm path length quartz cells and analyzed onboard with a UV-VIS diode array spectrophotometer (Ocean Optics USB 2000+, DT-mini 2000) using 2 mM unpurified m-Cresol Purple indicator (Aldrich, product no. 211761, lot no. MKBH6858V). Seawater pH (in the total hydrogen ion scale) was calculated at 25°C using Clayton and Byrne (1993) equations and taking into account the pH disturbance of m-Cresol Purple (Dickson et al., 2007). Precision of the pH measurements, through pooled standard deviation of replicate samples collected from the same Niskin bottle, was better than ±0.004 pH units. For quality control purposes, regular measurements of Tris buffer (lot no. 180 for VA-01/19 and lot no. 185 for VA-12/19, provided by Dr. Andrew Dickson, UC San Diego) were performed. For further calculations, pH was recasted to the *in situ* temperature and pressure according to Lui and Chen (2017). These estimations were in line with those estimated with the pHinsi function of the R seacarb package (version 3.2.13; Gattuso et al., 2020) at depths where both pH and TA were measured (r^2 = 0.999; RMSE=0.002 pH units; n=31). Hereinafter the term pH is used to refer to the *in situ* pH values.

TA samples were collected in 500 mL borosilicate glass bottles following Dickson et al. (2007) and stored in the dark at 10 °C until analysis. VA-01/19 cruise samples were

analyzed using the Astor et al. (2005) modification of the spectrophotometric method with bromocresol green indicator (Breland and Byrne, 1993). VA-12/19 cruise samples were determined by potentiometric titration with an open cell system based on Millero et al. (1993). The precision of the TA measurements, through pooled standard deviation of replicate analyses from a single sample was 5 µmol kg^{-1} for VA-01/19 and 3 µmol kg^{-1} for VA-12/19. The consistency of the TA measurements was carried out by comparison of pooled standard deviation of CRM measurements regarding its nominal value (Batch 179 for VA-01/19 and Batch 185 for VA-12/19, provided by Dr. Andrew Dickson, UC San Diego). Standard uncertainty of the CRM was 1.6 µmol kg^{-1} for VA-01/19 and 1.4 µmol kg^{-1} for VA-12/19.

DIC was estimated for each AT-pH pair using the carb function of the R seacarb package, considering the measured phosphate and silicate concentrations. The carbonic acid dissociation constants used were those given by Lueker et al. (2000), while hydrogen fluoride and hydrogen sulfate constants were those of Dickson and Goyet (1994) and Dickson (1990), respectively. For total boron concentration, Uppström (1974) formulation was selected. The propagated standard uncertainties in the estimated DIC, calculated with the seacarb errors function, was 5.1 µmol kg^{-1} for VA-01/19 and 3.4 µmol kg^{-1} for VA-12/19. The carbonate system buffer sensitivities $\partial pH/\partial TA$ and $\partial pH/\partial DIC$ acid-base buffer factors, which express the change in pH relative to a change in TA and DIC, respectively (Weber and Stumm, 1963; Frankignoulle, 1994), and the Revelle factor, the ratio of the fractional change in pCO_2 relative to the fractional change in DIC (Sundquist et al., 1979) were calculated with the seacarb buffergen function.

Chla samples were collected in dark bottles and filtered through glass fiber filters (GF/F grade). Filters were kept at -86 °C until analysis with a Perkin Elmer LS3 spectrofluorometer using the Lutz et al. (2010) modification of the Holm-Hansen et al. (1965) method. Seapoint *in vivo* fluorescence profiles were converted into Chla by calculating a Chla-fluorescence ratio at depths where Chla samples were analyzed and linearly interpolating the Chla-fluorescence ratios between these points.

Bacterioplankton samples were fixed with 2% v/v formaldehyde, stained with DAPI and filtered through 0.22 µm pore size black polycarbonate filters, following Porter and Feig (1980). Filters with the retained bacteria were preserved at -20°C until on land epifluorescence microscopy analysis. Abundances and cell volume, calculated according to

Jones (1979) and Bratbak (1985) respectively, were later used to estimate carbon biomass by the allometric function between carbon content and cell volume as proposed by Loferer-Krößbacher et al. (1998) and Posch et al. (2001).

Phytoplankton and protozooplankton samples were preserved with 20% v/v formaldehyde and qualitative-quantitative analyzed by the inverted microscope sedimentation method (Edler and Elbrächter, 2010). In addition, samples were collected to study the picoplankton fraction. For this purpose, dually stained samples with DAPI and Proflavin were filtered through 0.22 µm pore size black polycarbonate filters; filters were then stored at -20°C until on land analysis under an epifluorescence microscope (Booth, 1993). Phytoplankton and protozooplankton carbon biomass were calculated from biovolume formulations (Hillebrand et al., 1999) and group specific carbon-to-volume ratios (Putt and Stoecker, 1989; Booth, 1993; Menden-Deuer and Lessard, 2000). Phytoplankton and protozooplankton groups were classified according to their size (pico- <2 µm, nano- 2-20 µm and micro- 20-200 µm, Sieburth et al., 1978) and trophic modality (autotrophs or heterotrophs, the latter including mixotrophs or functional autotrophs ciliates).

2.4. Continuous underway system

Sea surface (~5 m depth) temperature and conductivity were continuously recorded along the cruise track with a Seabird SBE 38 thermographer and a Seabird SBE 45 thermosalinograph. Simultaneously, DO (Aandera Optode 3835), *in vivo* fluorescence (Wetlabs Wetstar) and seawater and air CO_2 dry molar fractions (xCO_2), were also measured. Underway DO and *in vivo* fluorescence-based estimates of Chla were obtained following the same procedure used for the vertical properties. xCO_2 was determined with a General Oceanics Inc. 8050 pCO_2 system equipped with a LI-COR 7000 nondispersive infrared detector. A sequence of seawater and air xCO_2 measurements was made every 2 minutes, with xCO_2 in air measured at 3-hour intervals. The LI-COR was calibrated every 3 hours using 0, 201.26, 399.68 and 598.18 ppm CO_2 standard gases (Air Liquide). CO_2 fugacities (fCO_2, the pCO_2 corrected for nonideality) in surface seawater (fCO_2sw) and air (fCO_2air) were computed from the xCO_2 data according to Takahashi et al. (2009) and following Pierrot et al. (2009) quality control procedures. The accuracy of the fCO_2 measured data was within 2 µatm.

2.5. Data analysis and visualization

A value of 50 J m^{-3} for the Simpson parameter was adopted following Kahl et al. (2017), for defining the location of the Mid-shelf front, separating the vertical stratified (>50 J m^{-3}) and mixed (<50 J m^{-3}) waters. The surface mixed layer, where turbulent mixing processes form an upper density layer distinct from the layer below, was defined for each profile by finding the depth with Brunt-Väisälä maximum water column buoyancy frequency (N^2max, Carvalho et al., 2017). This criterion was selected to better reflect mixed layer estimates by visual inspection of the individual profiles.

Two-way Permutational Multivariate Analysis of Variance (PERMANOVA) was used to examine differences in profile data between the two cruises and the COSTAL-AR stations. Spearman correlations were used as a measure of variables association. Principal component analysis (PCA) and hierarchical clustering analysis were used to explore patterns in the thermohaline, chlorophyll a and dissolved oxygen vertical properties along the COSTAL-AR section. PCA provided a set of low dimensional features from the vertical properties. Principal components were selected by the Kaiser Criterion (1960). Significances between a variable and a particular principal component were tested under the Broken Stick model (Peres-Neto et al., 2003). The distribution of clusters, determined by the NbClust majority rule (Charrad et al., 2014), was implemented to differentiate regions along the COSTAL-AR section by gathering cluster's shared stations. Wilcoxon Rank Sum test and Kruskal-Wallis test were used to check for differences among groups.

Differences between fCO_2sw and fCO_2air ($dfCO_2$ sea-air = fCO_2sw - fCO_2air) were obtained from the fCO_2sw data averaged in 5-minute intervals and a fCO_2air value of 410.1 µatm, calculated as the average of fCO_2air for the whole records in both cruises (401.4 µatm in VA-01/19 and 418.9 µatm in VA-12/19). The spatial and temporal coverage of the data was not sufficient to calculate a meaningful flux for the region, hence, $dfCO_2$ sea-air was used to provide an indication of the potential of surface waters to act as a CO_2 sink ($dfCO_2$ sea-air <0) or source ($dfCO_2$ sea-air >0).

The Takahashi et al. (2002) approach was used to assess the relative importance of the thermal and non-thermal effects on the changes of fCO_2sw. The temperature effect (Therm) on the observed fCO_2sw was calculated by perturbing the mean local fCO_2sw value by the difference between the observed and the mean temperature in the region of study. The non-thermal effect (Non-Therm), which represent the variability in fCO_2sw due to

changes in DIC and/or TA driven by the vertical mixing and/or biological utilization of CO_2 was addressed by normalizing the observed fCO_2sw values to the local mean temperature in the region of study. In both Therm and Non-Therm calculations, the Takahashi et al., 1993 temperature effect correction on fCO_2sw for isochemical seawater ($\partial \ln pCO_2sw/\partial$ temperature = 0.0423 $°C^{-1}$) was applied. To assess the relative importance of Non-therm effects on the changes of fCO_2sw, the ratio of the Non-therm over the Therm amplitudes (BT_A = $Non\text{-}therm_A/Therm_A$) was computed. A BT_A ratio >1 indicates that the non-thermal effects (e.g. biological utilization of CO_2) prevail over the thermal effects (and hence dominate the variability), while a BT_A ratio <1 indicates that the non-thermal effects are weaker. A spatial subdivision along the COSTAL-AR section was considered in the analysis. For this purpose, the binary segmentation method (Scott and Knott, 1974) for change point detection was implemented to differentiate regions by changes in mean and variance within the fCO_2sw underway data.

TA-salinity and TA-DIC relationships were explored to assess possible causes of TA and DIC variability. The TA-salinity and TA-DIC least square regressions were computed on the basis of the observations made in the first 50 meters. The changes in TA arising from hydrological and biological effects were accounted for when analyzing the salinity dependence on TA. The hydrological effects of seawater dilution and evaporation on TA were removed by normalizing each TA value to a salinity of 35 (NTA=TA 35 / salinity; Millero et al., 1998). The biological effects on TA induced by nutrient cycling were considered relative to nitrate changes and the proportional uptake of phosphate and sulphate, by including the Redfield ratio of 1.36 (Wolf-Gladrow et al., 2007). Herein after the biological effects on TA are referred as potential TA (PTA, expressed as PTA = TA + 1.36 nitrate).

Statistical analysis, figure subpanels and maps were produced using R project (R Core Team, 2021) and Ocean Data View (Schlitzer, 2021) free software. Map interpolations were made to provide reader-friendly visualization of the results. Data Interpolating Variational Analysis was used to ensure data structure preservation. A list of acronyms and symbols used in the text is presented in table A2.

3. RESULTS

3.1. Distribution of thermohaline properties, chlorophyll a and dissolved oxygen

Subantarctic Shelf Water dominated the COSTAL-AR section (figure 2), with relatively low salinity middle shelf waters (33.5-33.7) resulting from the contribution of diluted waters by continental runoff (Lusquiños and Valdéz, 1971). During the VA-01/19 cruise, relatively high salinity waters (>33.8) were found at coastal stations (Guerrero and Piola, 1997; Lucas et al., 2005). No influence of La Plata River waters was detected during these cruises. The thermal Mid-shelf front was evident in both cruises near the 50 m isobath, offshore station CT1 during the VA-01/19 and offshore station CT2 during the VA-12/19 cruise, according to the Simpson parameter. Stratification was stronger during the VA-01/19 cruise. Three systems were identified along the COSTAL-AR section according to the profiles that shared the same cluster groups (Figure A1): a coastal system mostly vertically homogeneous in temperature and salinity, a stratified shelf system with a deep Chla maximum and relatively high values of Chla at surface onshore of the Shelf-break front, and a shelf-break system with lower Chla towards offshore. Additional result analysis from cluster analysis are detailed in supplementary material.

During the VA-01/19 cruise a marked thermocline was observed in the shelf at ~30 m depth (stations CT2 to CT5; figure 2, left). In the surface mixed layer, temperature dropped gradually from the coast, with values just above 20 °C, to 18.1 °C in the outer shelf; Chla and DO values of 1.5 mg m^{-3} of 269 µmol kg^{-1}, respectively were found the middle shelf (station CT4). In the outer shelf (station CT5), where a notable elevation of the isotherms to ~20 m indicated an upwelling of slope waters, underway data showed higher values of Chla (2.2 mg m^{-3}; also captured by the satellite-based Chla estimations at the time of the cruise; figure 1, center) and DO (281 µmol kg^{-1}). Just below the mixed layer (~35 m), values as high as 14.2 mg m^{-3} of Chla and 388 µmol kg^{-1} of DO were observed in the middle and outer-shelf. These features were followed by a prominent thermohaline gradient of the Shelf-break front, reaching salinity values of 34.4 and a sharp shift of Chla and DO towards minimum values (0.3 mg m^{-3} and 266 µmol kg^{-1}, respectively) at the outer and deeper station (CT6). A complex thermohaline profile was observed at station CT6, with the presence of slope waters from the Malvinas Current and waters from the Brazil Current (Piola et al., 2000, 2010; Piola and Matano 2001).

During the VA-12/19 cruise the thermocline was observed in the middle shelf at around 35-40 m depth (stations CT3 and CT4; figure 2, right). In the top 30 m of the water column, the temperature decreased gradually from 16.3 °C at the coast, to 8.9 °C in the outer shelf. Stations CT1 to CT3 presented fairly constant water column Chla and DO values (1.1 mg m^{-3} and 271 µmol kg^{-1}, respectively), while the highest values of Chla (3.2 mg m^{-3}) and DO (290 µmol kg^{-1}) were observed above the thermocline in the middle and outer shelf (station CT4; also captured by the satellite-based Chla estimations at the time of the cruise; figure 1, right). The Shelf-break front signal was detected at station CT5, where high values of Chla (2.9 mg m^{-3}) and DO (340 µmol kg^{-1}) were found throughout the top 30 m. At station CT6 slope waters (salinity ~34.2, temperature <10 °C) dominated the upper profile, with relatively high Chla (1 mg m^{-3}) and (306 µmol kg^{-1}) DO values.

PERMANOVA analysis from vertical properties data showed a significant cruise-station interaction (p-value <0.001) between the two cruises. During the VA-01/19 cruise the top most significantly correlated variables (Spearman correlation coefficients; p-value <0.001) were temperature-depth (-0.78), DO-depth (-0.65), temperature-DO (0.49), DO-Chla (0.40) and Chla-depth (-0.39). Three principal components (PC) were selected, accounting for a cumulative explained variance of 93% (figure 3, left). Both DO and Chla had a significant contribution to PC1, a component that can be associated with biological activity, while temperature and salinity had their main contribution to PC2 and PC3, respectively. In comparison, during the VA-12/19 cruise the most significantly correlated pairs of variables were Chla-depth (-0.79), temperature-depth (-0.77), salinity-DO (0.70) and Chla-temperature (0.57). Two PCs were selected, accounting for a cumulative explained variance of 82%. Temperature and Chla had a significant contribution to PC1, a component that can be associated with warmer, seasonally stratified and productive shelf waters, while DO and salinity had their main contribution in the PC2, related to slope waters (figure 3, right).

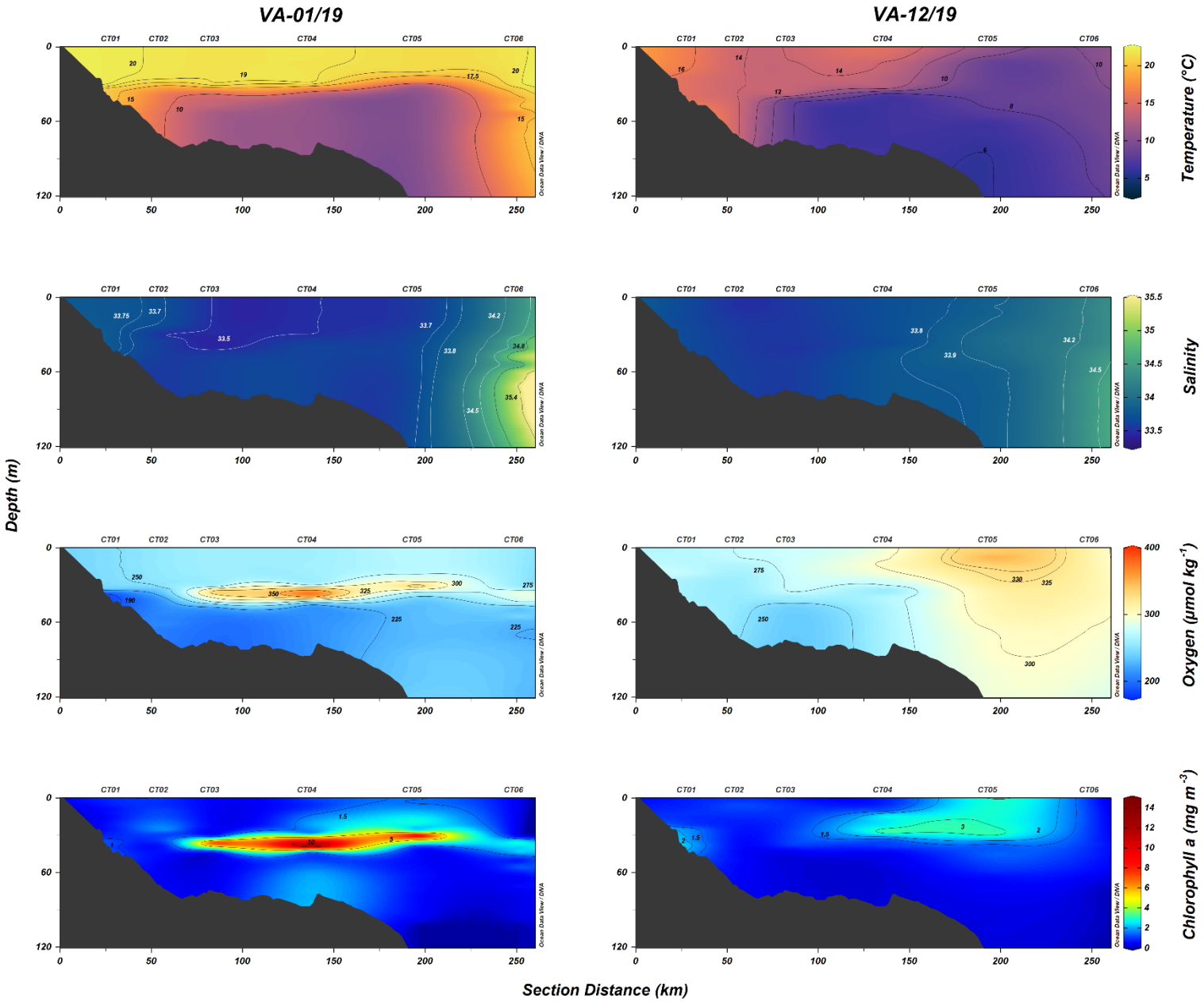

Figure 2. Vertical properties (y-axis) of temperature (°C), salinity, dissolved oxygen (µmol kg^{-1}) and chlorophyll a (mg m^{-3}) in the top 120 meters along the COSTAL-AR section distance (Km; x-axis) during summer. Left: VA-01/19 cruise; right: VA-12/19 cruise.

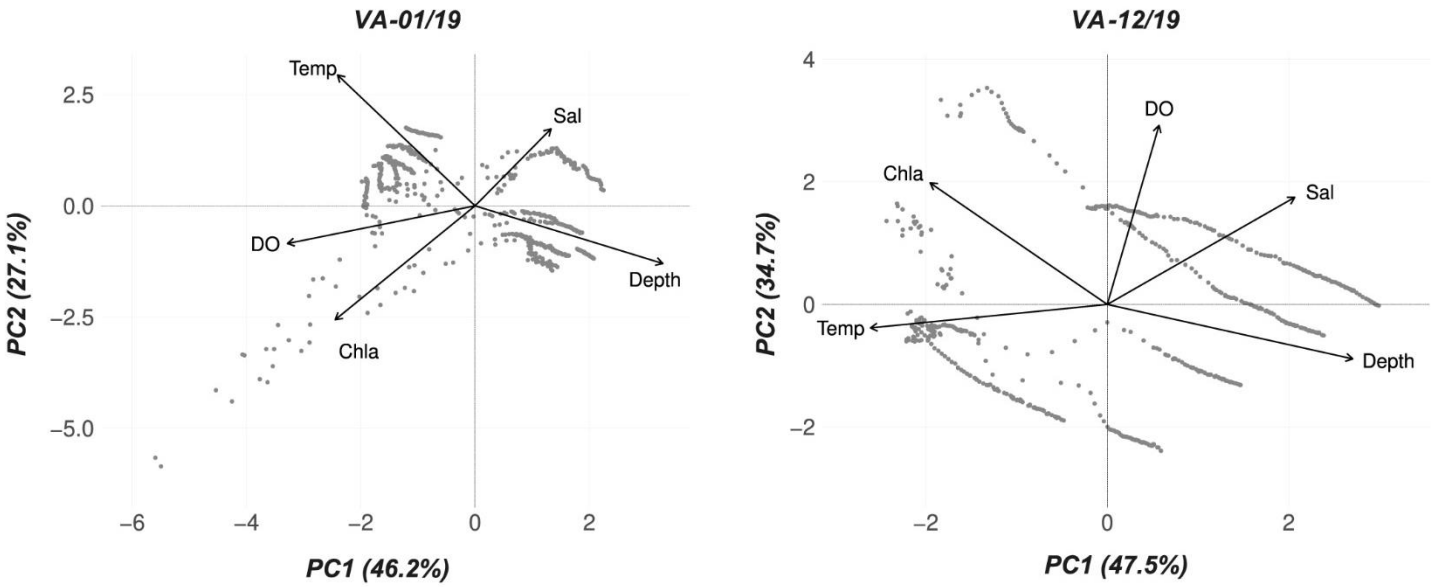

Figure 3. Principal component analysis biplot of temperature (Temp, °C), salinity (Sal), depth (m), dissolved oxygen (DO, µmol kg^{-1}) and chlorophyll a (Chla, mg m^{-3}) along the COSTAL-AR section during summer, showing the first two principal components (PC1-PC2), with both loadings of variables (vectors) and PC scores (dots) of profile observations. Left: VA-01/19 cruise; right: VA-12/19 cruise.

3.2. fCO_2 underway data

Three systems were also observed from the distribution of underway fCO_2sw along the COSTAL-AR section (figure 4): a coastal system (<60 km from the coast), a shelf system (between 60 and 240 km), and a shelf-break system (>240 km from the coast); its limits closely match the location of the Mid-shelf front and Shelf-break front. On each system the two cruises showed significant differences in fCO_2sw (Wilcoxon and Kruskal-Wallis tests; p-value <0.05). High average fCO_2sw values were observed in both cruises on the coastal system, though spatial variations occurred on the shelf (figure 4 and table 1). During the VA-01/19 cruise, fCO_2sw values decreased towards the middle and outer shelf until reaching a minimum on the onshore side of the Shelf-break front (282 µatm; station CT5 area). Offshore side of the Shelf-break front, high values about 315 µatm were found. During the VA-12/19 cruise, fCO_2sw values decreased towards middle shelf until reaching a minimum (216 µatm; station CT3 area); then values increased until reaching higher values (360 µatm) on the offshore side of the Shelf-break front.

Overall, the COSTAL-AR section in summer was likely a sink of CO_2 (average $dfCO_2sea$-air for the whole section were -87 ± 46 µatm in VA-01/19 and -112 ± 47 µatm in VA-12/19). During the VA-01/19 cruise, the coastal region was likely a weak source of CO_2 to the atmosphere, and a change to a CO_2 sink occurred near the 50 m isobath, related with the Mid-shelf front (figure 4 and table 1). During the VA-12/19 cruise, although absorption was lower at the coast, the entire section was likely a sink of CO_2. In both cruises the shelf was likely the region of strongest sink of CO_2 (table 1).

The analysis of the relative importance of thermal and non-thermal effects on the fCO_2sw revealed that all systems in both cruises presented BT_A ratios >1 (table 1). Hence, non-thermal effects (e.g. biological utilization of CO_2) dominated the fCO_2sw variability along the COSTAL-AR section during summer. A high spatial variability on both non-thermal and thermal effects was observed along the cruise track (figure 5), though signals in each cruise behaved differently. In particular, notable differences were found in the coastal system and shelf system, where the estimated BT_A ratios were nearly three and 1.3 times higher, respectively during the VA-12/19 cruise. In contrast, the shelf-break during the VA-01/19 cruise presented BT_A values 1.2 times higher than the VA-12/19 cruise.

With the aim of exploring the non-thermal effects acting on the fCO_2sw variability along COSTAL-AR section, underway fCO_2sw records were plotted together with

temperature, salinity and Chla (figure 6). In both cruises changes in mixing (coastal system) and stratification (shelf system) possibly had an influence on the fCO_2sw values. Evidence of fCO_2sw variability due to biological utilization of CO_2 was also found in both cruises. During the VA-01/19 cruise (figure 6, top), fCO_2sw substantially decreased onshore side of the Shelf-break front (CT5 area) when both Chla and DO exhibited their maxima (2.2 mg m^{-3} and 281 µmol kg^{-1}, respectively). During the VA-12/19 cruise (figure 6, bottom), fCO_2sw reached a minimum value in an area of the middle shelf, where both Chla and DO had high values (~2.5 mg m^{-3} and 280 µmol kg^{-1}, respectively). During this cruise the fCO_2sw spatial variability towards the outer shelf was related to the prevalence of high salinity slope waters. In both cruises the thermohaline gradient of the Shelf-break front dominated the fCO_2sw spatial variability.

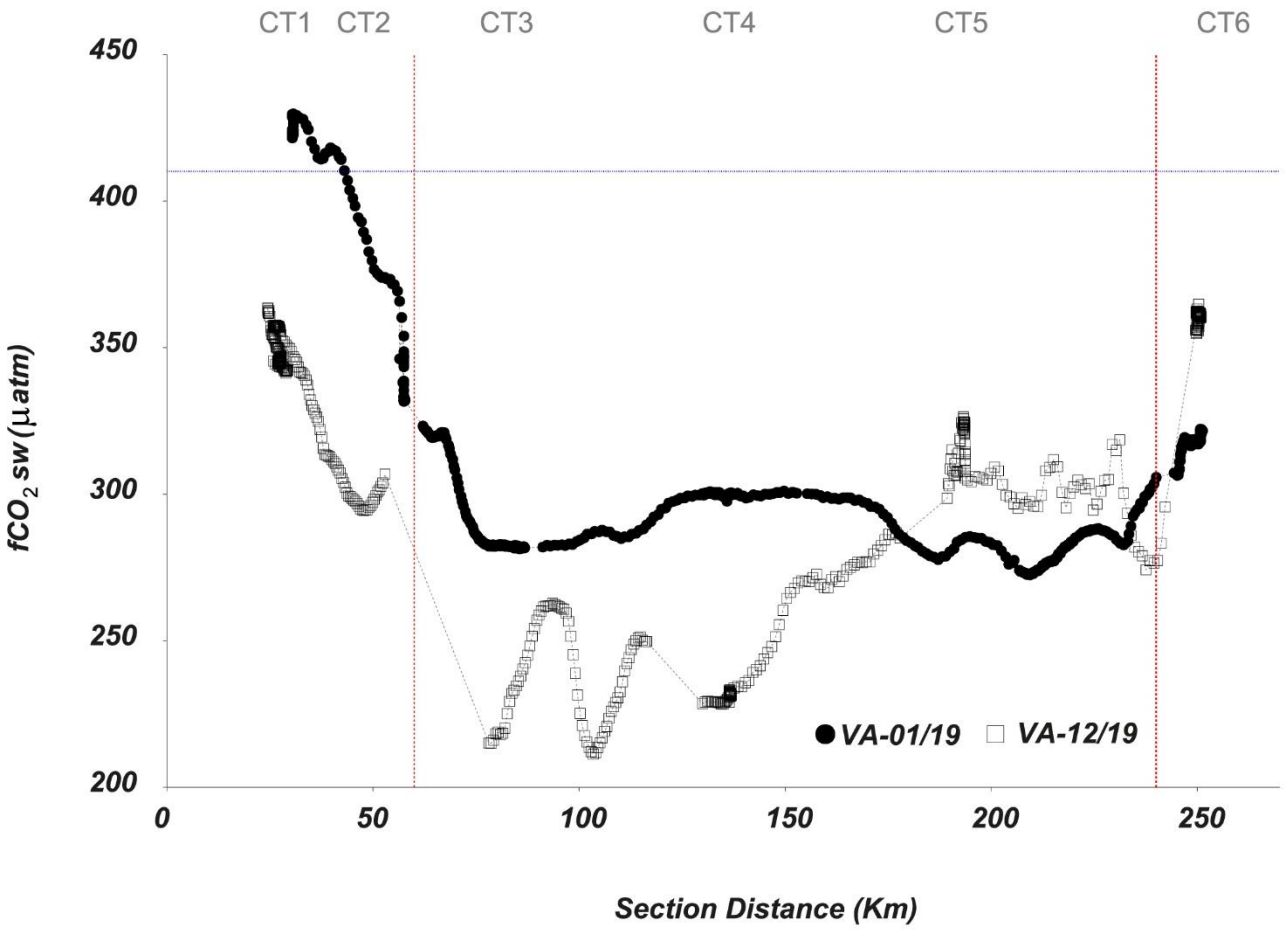

Figure 4. Underway fCO_2sw (µatm; y-axis) along the COSTAL-AR section distance (Km; x-axis) during summer. VA-01/19 cruise is shown with filled circles; VA-12/19 cruise is shown with open squares. The horizontal dotted line represents the average fCO_2air (410.1 µatm) for both cruises. Values of fCO_2sw below this line indicate negative $dfCO_2$ sea-air values. The vertical dotted red line separate the main oceanographic systems established by the change point method (see main text). Station positions are also indicated.

Table 1. Underway surface data (mean ± SD) of temperature (Temp, °C), salinity (Sal), fCO_2sw (µatm), $dfCO_2$ sea-air (µatm), dissolved oxygen (DO, µmol kg^{-1}), chlorophyll a (Chla, mg m^{-3}) and the relative importance of the non-thermal and thermal effects on the changes of fCO_2sw along the different systems in COSTAL-AR section during the two summer cruises. The non-thermal and thermal effects are expressed in terms of their amplitudes (Non-$therm_A$ and $Therm_A$, respectively; µatm) with their corresponding non-thermal-to-thermal ratios (BT_A = Non-$therm_A$/$Therm_A$). The amplitudes in temperature ($Temp_A$, °C) and fCO_2sw (fCO_2sw_A, µatm) are also presented. n: number of observations.

	VA-01/19											
	Temp	*Sal*	*fCO_2sw*	*$dfCO_2$ sea-air*	*DO*	*Chla*	*$Temp_A$*	*fCO_2sw_A*	*Non-$therm_A$*	*$Therm_A$*	*BT_A*	*n*
Coastal	20.16 ± 0.4	33.72 ± 0.04	393.4 ± 37	1.0 ± 37	259.0 ± 4	0.9 ± 0.0	1.0	98.1	83	17.1	4.9	101
Shelf	19.09 ± 0.5	33.54 ± 0.1	291.2 ± 11	-108.4 ± 14	272.0 ± 5	0.9 ± 0.4	1.5	50.8	38.8	18.7	2.1	355
Shelf-Break	19.57 ± 0.1	34.24 ± 0.09	317.7 ± 4	-97.9 ± 4	268.3 ± 4	0.5 ± 0.1	0.3	15.8	11.8	4.4	2.7	109

	VA-12/19											
	Temp	*Sal*	*fCO_2sw*	*$dfCO_2$ sea-air*	*DO*	*Chla*	*$Temp_A$*	*fCO_2sw_A*	*Non-$therm_A$*	*$Therm_A$*	*BT_A*	*n*
Coastal	16.43 ± 0.1	33.61 ± 0.03	339.7 ± 20	-97.0 ± 22	244.0 ± 3	1.1 ±0.3	0.4	69.1	71.0	5.3	13.4	191
Shelf	13.22 ± 2	33.71 ± 0.09	266.5 ± 36	-140.4 ± 46	281.5 ± 17	1.6 ± 0.7	5.5	115.1	166.1	60.5	2.7	271
Shelf-Break	10.38 ± 0.1	34.21 ± 0.03	360.5 ± 2	-55.3 ± 9	278.1 ± 1	1.1 ± 0.3	0.3	10.1	10.7	4.8	2.2	82

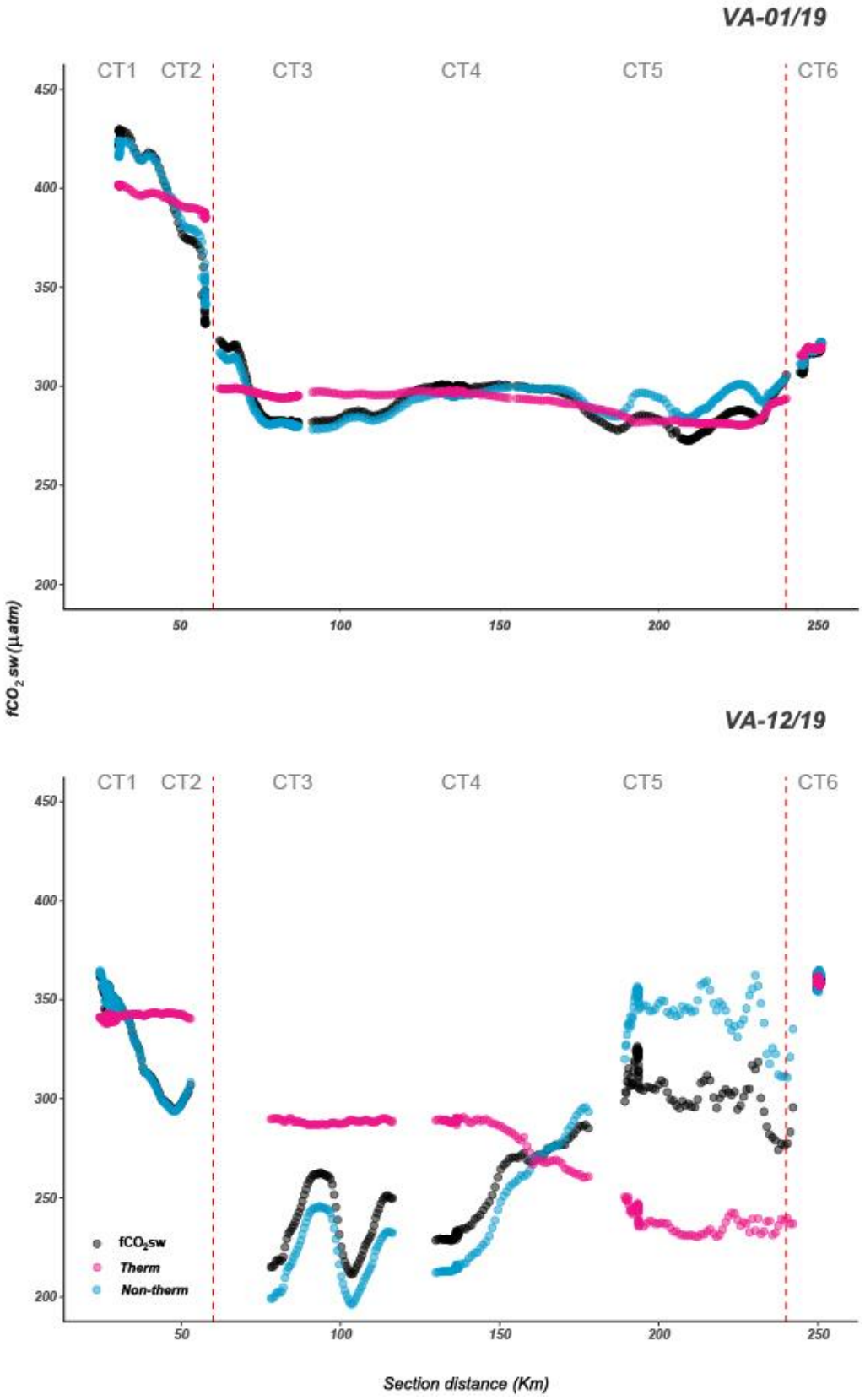

Figure 5. Thermal and non-thermal effects on the fCO_2sw (µatm; y-axis) along the COSTAL-AR section distance (Km; x-axis) during summer. The vertical dotted red line separate the main oceanographic systems established by the change point method (see main text). Top: VA-01/19 cruise; bottom: VA-12/19 cruise. Station positions are also indicated.

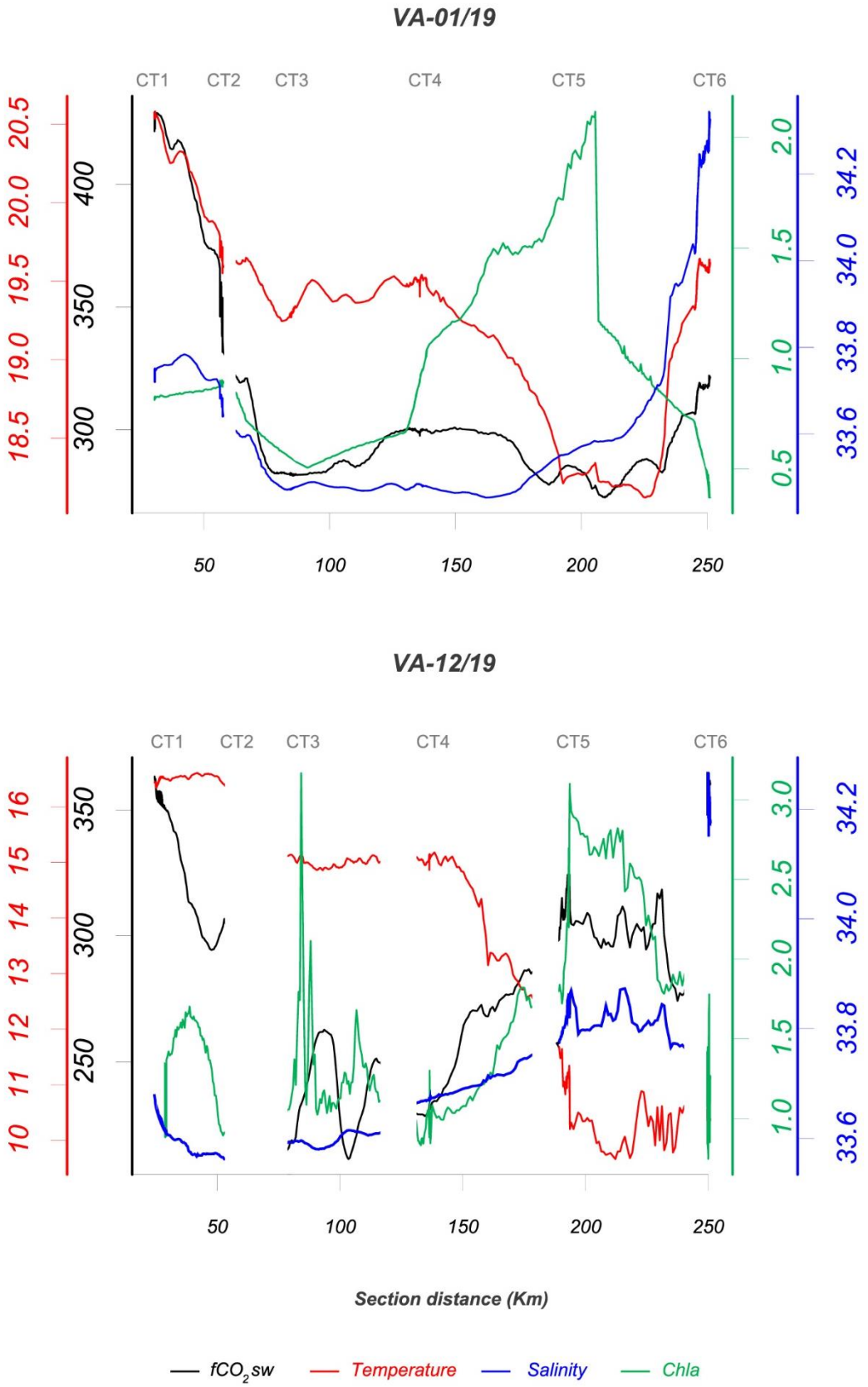

Figure 6. Underway records (y-axis) of fCO_2sw (µatm; black), temperature (Temp, °C; red), salinity (Sal; blue) and chlorophyll a (Chla, mg m^{-3}; green) along the COSTAL-AR section distance (Km; x-axis). Top: VA-01/19 cruise; bottom: VA-12/19 cruise. Station positions are also indicated.

3.3. Vertical distribution of carbonate system and nutrients

In both cruises, high pH values of 8.15 (VA-01/19) and 8.19 (VA-12/19) were found above the thermocline in the middle shelf (figure 7, top); lower pH values (~7.9) were registered at deeper depths. Slope waters were associated with pH values of 8.07. Average TA values for all sampled stations at all depths were 2264 ± 40 µmol kg^{-1} (VA-01/19; n=19) and 2266 ±14 µmol kg^{-1} (VA-12/19; n=12). In both cruises, high TA values approaching 2300 µmol kg^{-1} were associated with slope waters (figure 8, left). A horizontal decreasing DIC gradient was observed at the surface mixed layer from the coastal stations towards the middle shelf. DIC values of 1949 µmol kg^{-1} (VA-01/19) and 1963 µmol kg^{-1} (VA-12/19) were estimated above the thermocline in the middle shelf. Higher DIC values about 2154 µmol kg^{-1} (VA-01/19) and 2139 µmol kg^{-1} (VA-12/19) were estimated near the bottom in the mid-outer shelf, the latter associated with slope waters. Carbonate system buffer sensitivities in the top 50 m for the whole COSTAL-AR section were ~1850 (mol kg^{-1})$^{-1}$, -2000 (mol kg^{-1})$^{-1}$ and 11, for the acid-base buffer factors ∂pH/∂TA and ∂pH/∂DIC and the Revelle factor, respectively. Relatively low nitrate concentrations were found above the thermocline, with average values of 0.07 ± 0.04 µmol kg^{-1} during the VA-01/19 cruise and higher values of 0.14 ± 0.12 µmol kg^{-1} during the VA-12/19 cruise. In both cruises higher nitrate concentrations (>6 µmol kg^{-1}) were found associated with slope waters. The distribution of phosphate and silicate resembled that of nitrate. Average values of carbonate system and dissolved inorganic nutrient data for the coastal, shelf and shelf-break systems are presented in table A3.

The TA-salinity and TA-DIC regressions in the top 50 m (n=21; figure 8) for the two cruises together were TA= 50.1 salinity + 577.4 (r^2 =028; RMSE=31) and TA= 0.45 DIC + 1349 (r^2 =0.67; RMSE=21.1), respectively. During the VA-01/19 cruise, conspicuous high values of TA (2386 µmol kg^{-1}) and DIC (2228 µmol kg^{-1}) were found near the bottom in the shallower coastal station, associated with a high nitrite concentration (0.64 µmol kg^{-1}) and low values of pH and DO (7.80 and 198 µmol kg^{-1}, respectively). By excluding this value, the TA-salinity and TA-DIC regressions (n=20) improved their fitting with TA= 51.2 salinity + 534.2 (r^2 =0.65; RMSE=15.2) and TA= 0.33 DIC + 1603 (r^2 =0.41; RMSE=19.6), respectively. When the hydrological and biological effects were addressed on TA (i.e. salinity normalized TA, NTA and potential TA, PTA), fairly uniform TA values resulted and the NTA-salinity and PTA-salinity relationships were neither well correlated nor significant, suggesting that the effects

of the processes causing TA variation along the COSTAL-AR section have been successfully removed. Regarding the TA-salinity relationships for the whole top 50 m data, there was a marked difference in between cruises (figure 8; table A4). During the VA-01/19 cruise seawater dilution and evaporation effects did not have a strong influence on TA (TA-salinity least squares regression coefficient was r^2 = 0.27). On the contrary, during the VA-12/19 cruise it seemed evident the major salinity effect on TA (TA-salinity least squares regression coefficient was r^2 = 0.76). Finally, in the TA-DIC diagram (figure 8, right) all data (except one point) lye above the theoretical seawater dilution and evaporation line. We can speculate that the mayor effects affecting the TA-DIC relationship would be biological.

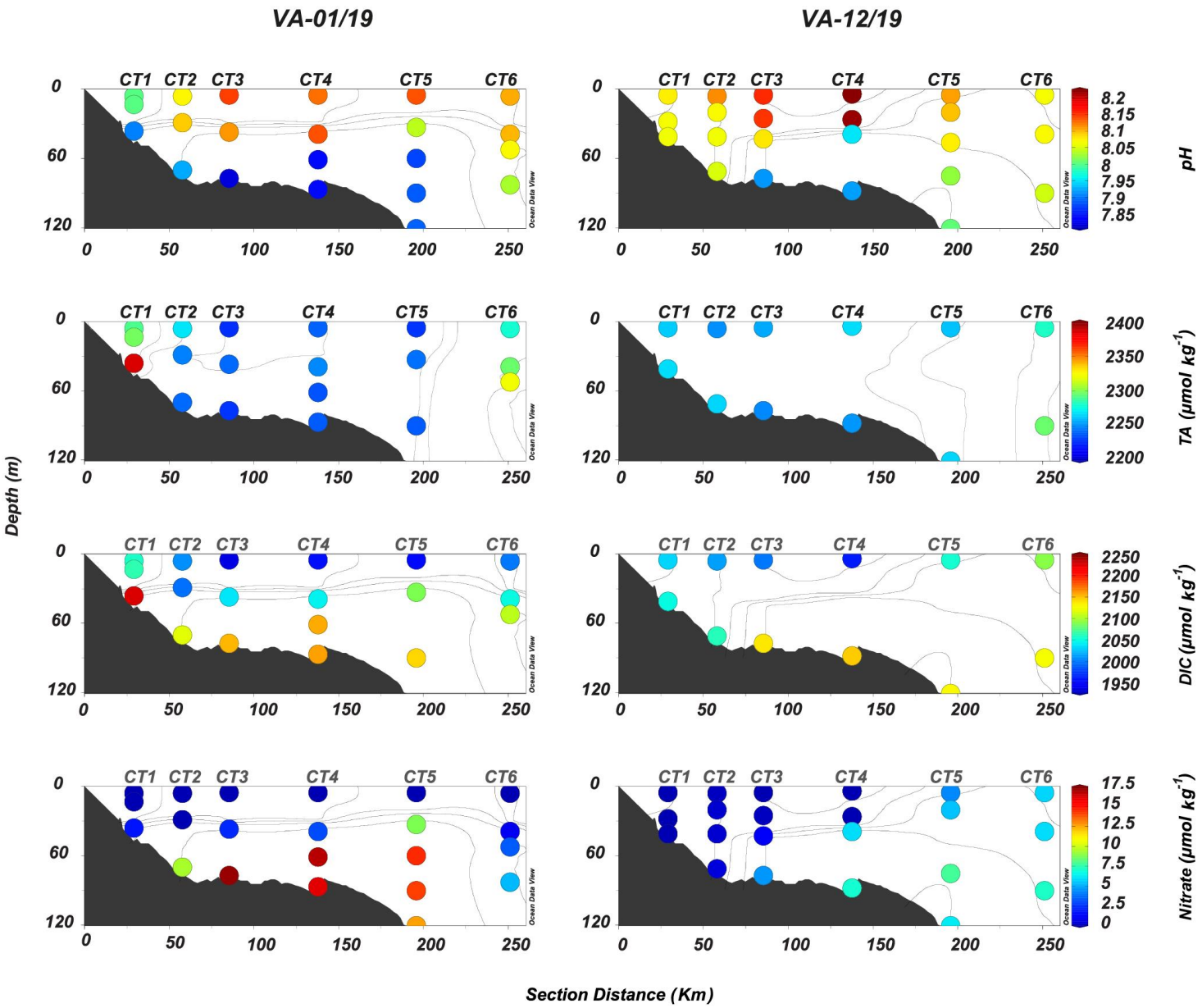

Figure 7. Vertical properties (x-axis) of pH, total alkalinity (TA, µmol kg^{-1}), dissolved inorganic carbon (DIC, µmol kg^{-1}) and nitrate concentration (µmol kg^{-1}) in the top 120 meters along the COSTAL-AR section distance (Km; x-axis). Left: VA-01/19 cruise; right: VA-12/19 cruise. Color-coded circles representing magnitude of these properties are superimposed on temperature contours, except for TA that is plotted on salinity contours. Station positions are also indicated.

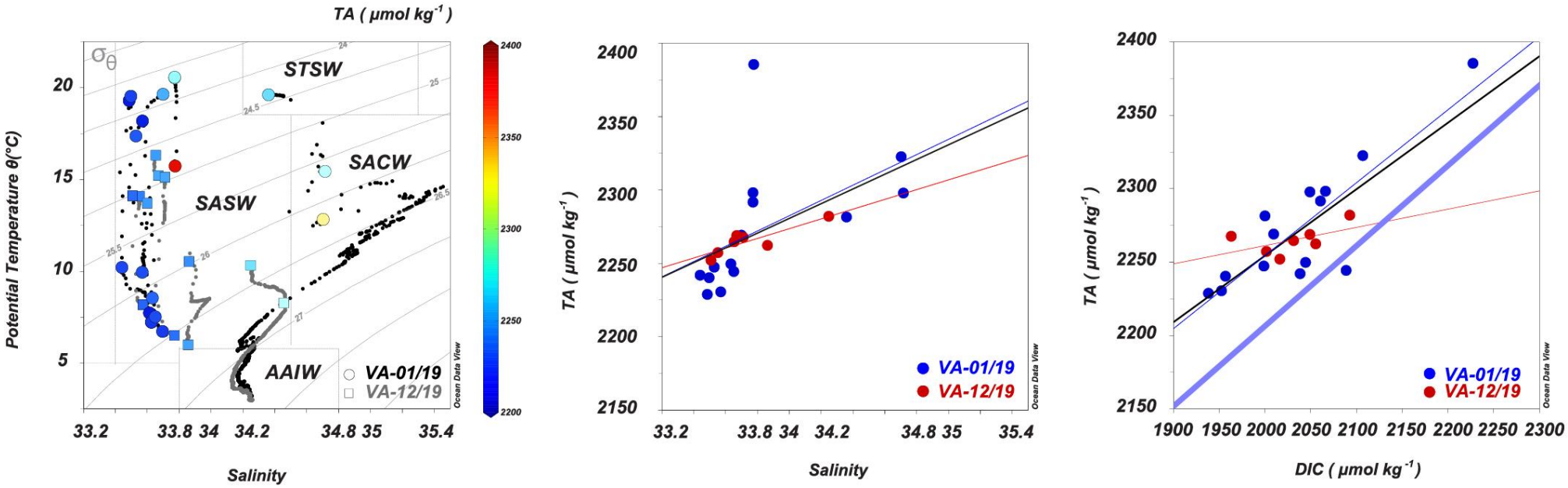

Figure 8. Left: Potential temperature (θ, °C) versus salinity property-property diagram for the VA-01/19 (blue dots) and VA-12/19 (red dots) cruises at all depths (950 m). Color-coded VA-01/19 (circles) and VA-12/19 (squares) representing the magnitude of total alkalinity (TA, µmol kg^{-1}) samples collected in the top 50 m are superimposed to the θ-salinity property-property diagram. Isopycnals (σθ) and water masses (Möller et al., 2008) are indicated by grey lines and dotted line polygons, respectively. SASW: Subantarctic Shelf Water, STSW: Subtropical Shelf Water, SACW: South Atlantic Central Waters, AAIW: Antarctic Intermediate Waters. Center and right: property-property diagrams of total alkalinity (TA, µmol kg^{-1}) versus salinity and total alkalinity versus dissolved inorganic carbon (DIC, µmol kg^{-1}) for the samples collected (VA-01/19, blue; VA-12/19 red) in the top 50 m (n=21). Least square regression lines are also shown: black continuous line for the two cruises together; blue and red dashed lines for the VA-01/19 and VA-12/19 cruises, respectively. The light blue line in the right panel shows the theoretical effect of seawater dilution and evaporation process. See main text and table A4 for least square regression equations.

3.4. Microbial communities

Phytoplankton dominated the microbial community biomass throughout the top 50 meters of the COSTAL-AR section (figure 9). During the VA-01/19 cruise, the picophytoplankton *Synechococcus sp* dominated the mixed layer both in coastal (37 mg C m^{-3}) and shelf (45 mg C m^{-3}) stations. In the outer shelf (station CT5), a high phytoplankton biomass of 87 mg C m^{-3}, composed almost exclusively of the nanoplanktonic coccolithophore *Emiliania huxleyi* was found at the mixed layer. Below the mixed layer in the middle and outer shelf, a prominent maximum of up to 300 mg C m^{-3} biomass was found, which corresponded to tiny coccal phytoeukaryotes (2-3 µm diameter). On the offshore side of the Shelf-break front (station CT6) the autotrophic community was almost exclusively composed of *Synechococcus sp* (72 mg C m^{-3} at 39 m).

During the VA-12/19 cruise, the coastal station presented low phytoplankton biomasses at 5 m, composed mainly by micro and nano- dinoflagellates; near the bottom higher biomasses were found, composed by microplankton (67 mg C m^{-3}). *Synechococcus sp* dominated the shelf, with values >50 mg C m^{-3} and reaching bloom characteristics (230 mg C m^{-3}) in the middle shelf (station CT4). Dinoflagellates were also found in the middle shelf (~30 mg C m^{-3}). The outer shelf was dominated by non-calcareous haptophytes (~50 mg C m^{-3}); coccolithophorids were also found, with low biomasses (*E. huxleyi*, ~10 mg C m^{-3}). Non-calcareous haptophytes and coccolithophorids were also the main component at the outer and deeper station, although in low biomass (~20 mg C m^{-3} and ~5 mg C m^{-3}, respectively).

The microbial heterotrophic biomass in both cruises was largely dominated by the bacterioplankton. In both cruises high values of bacterioplankton biomass were found below the thermocline in the middle shelf (24.5 mg C m^{-3} during the VA-01/19 cruise and 88.0 mg C m^{-3} during the VA-12/19 cruise), in coincidence with the highest phytoplankton biomass. The protozooplankton was present in minor proportion in terms of biomass. During the VA-01/19 cruise consisted mainly of naked ciliates and to a lesser extent of dinoflagellates and other flagellates; during the VA-12/19 cruise presented slightly higher biomasses and were dominated by flagellate forms.

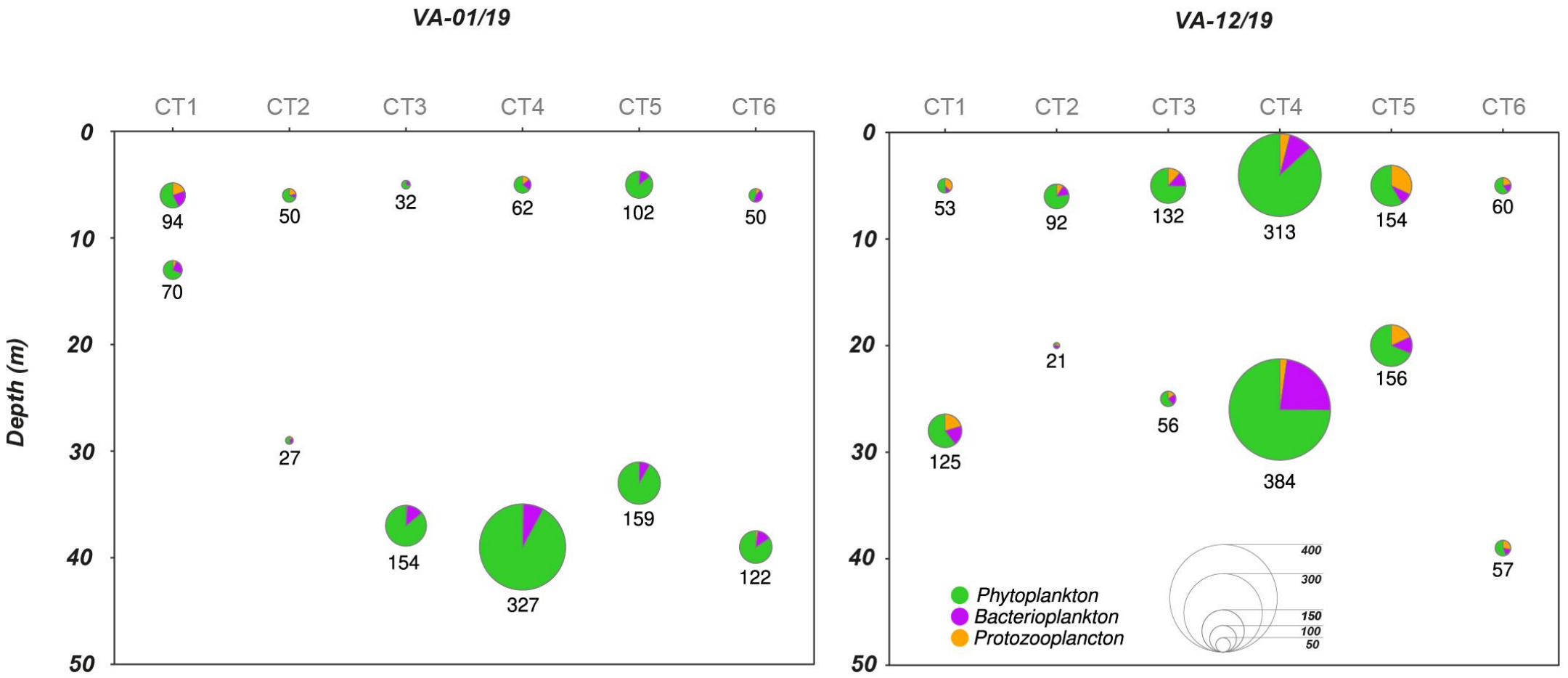

Figure 9. Pie charts of microbial community biomasses in the top 50 meters of the water column (y-axis), showing relative contributions of the phytoplankton (green), bacterioplankton (purple) and protozooplankton (orange) along the COSTAL-AR section (x-axis) during summer. Left: VA-01/19 cruise; right: VA-12/19 cruise. Size of pie charts and numbers below each pie chart denote the total biomass (mg C m^{-3}). Station positions are also indicated.

4. DISCUSSION

4.1. Processes affecting the distribution of the microbial communities

Shelf waters at temperate latitudes are characterized by the typical development and breakdown cycle of the seasonal thermocline that controls the availability of nutrients and light. As a result, patterns of phytoplankton are strongly regulated by changes in water column vertical stability (Sverdrup, 1953; Margalef, 1978). Along the COSTAL-AR section thermal stratification governed the transition from a coastal system vertically homogeneous in temperature and salinity, consistent with the mixing produced by winds and tides (Martos and Piccolo, 1988), and a shelf system with a typical summer stratification (figure 2). These transitions conditioned the distribution features of the microbial communities. The PCA analysis showed that Chla had a significant contribution to PC1 indicating its influence on the variability of the environmental data considered, which played in the same way in both cruises, i.e., a characteristic deep Chla maximum in the middle shelf system, an outer shelf system with relatively high values of Chla at surface onshore of the Shelf-break front and lower Chla towards offshore. This is in agreement with previous characterizations of the COSTAL-AR section (Lutz and Carreto, 1991; Carreto et al., 1995; Negri et al., 2016). The main difference between the two cruises had to do with the degree of advance in the summer season and the position of the Shelf-break front in relation to the influence of the slope waters on the shelf (Bianchi et al., 1982).

Cruise VA-01/19 took place in middle summer, when temperatures were higher, the thermocline was well developed along the shelf and only the most coastal region remained vertically homogeneous. Associated with the thermocline, a noticeable deep Chla maximum occurred (14.2 mg m^{-3}), which was dominated by tiny coccal phytoeukaryotes (300 mg C m^{-3}; figure 2). This kind of deep Chla maximum is typical in summer, when nutrients have been mostly consumed at the surface mixed layer and phytoplankton accumulates at the base of the mixed layer where they find a suitable compromise of light still reaching from above and nutrients being exchanged from below the seasonal thermocline (reviewed in Cullen, 2015). As it is well known, here picophytoplankton activity was associated with low nutrient concentrations found in the surface mixed layer (Chisholm, 1992; Marañon, 2015). The role of the Shelf-break front in favoring productive processes (Segura et al., 2013) was observed on the onshore side of the Shelf-break front, where Chla and DO had their highest values (2.2 mg m^{-3}, 281 µmol kg^{-1}) associated with a high biomass of the coccolithophorid *E.*

huxleyi. The upwelling of slope waters likely enhanced nutrient renewal on this frontal area (Carreto et al., 1995; Piola et al., 2010), contributing to the maintenance of *E. huxleyi*, a common feature of this region during summer (Brown and Yoder, 1994; Signorini et al., 2006; Garcia et al., 2008; Poulton et al., 2013; Balch et al., 2014). This bloom was well captured by satellite-based Chla and particulate inorganic carbon estimations at the time of the cruise (figures 1 and A3), the latter resulting from the coccoliths (calcium carbonate plates covering the cells).

Cruise VA-12/19, on the other hand, took place right at the beginning of summer, when the thermocline was only well developed in the middle shelf. Above the thermocline, relatively high Chla (~3 mg m^{-3}), high biomasses of *Synechococcus sp* (>230 mg C m^{-3}, figure 9) and slightly higher nutrient values were found in the middle and outer shelf stations (figure 7). The prevalence of high salinity and oxygenated slope waters (both properties had their main contribution to PC2 in the PCA analysis) transported from the Malvinas Current in the outer shelf and shelf break suggests a mechanism for the supply of nutrients. In accordance fairly high biomasses of non-calcareous haptophytes (~50 mg C m^{-3}) were found, matching relatively high nitrate values (>6 µmol kg^{-1}). These values are in line with nutrients previously reported in the area (Braga et al., 2008; Gonçalves-Araujo et al., 2012).

The microbial communities exhibit a vast diversity and play essential roles in marine food webs. *Synechococcus sp* and coccal picophytoeukaryotes, were the largest contributors to microbial carbon biomass along the COSTAL-AR section during summer. The significance of picophytoplankton summer production in the Argentine Continental Shelf (Silva et al., 2009, Antacli et al., 2018; Guinder et al., 2020) can be related to its large surface-to-volume ratio, which confers them a competitive advantage under limiting nutrient conditions (Chisholm, 1992; Raven, 1998). Although the evaluation of the role of the microbial heterotrophs in driving the breakdown and recycling of organic material is beyond the scope of this work, the close bacterial-phytoplankton dynamics found (in particular for the VA-12/19 cruise) reflects the trophic dependence of these microbial partners (Li, 1998). This suggests that remineralization and secondary production could be an important process affecting carbon flux along the COSTAL-AR section. We also speculate that the protozooplankton community found could be a key link between the small phytoplankton and the zooplankton (Cepeda et al., 2020).

4.2. Processes involved in the carbonate system variability

Continental shelves hold a CO_2 complexity that arises from a highly variable interplay of factors over time and space (Bauer et al. 2013; Gruber, 2015; Laruelle et al., 2014, 2017; Roobaert et al., 2019; Cao et al., 2020). Seasonally stratified shelf seas have been identified as providing an important sink for atmospheric CO_2 (Borges et al., 2005; Chen and Borges, 2009). Hence, better understanding the role that individual continental shelves play in the global carbon budget, and associated acidification problem, becomes presently more relevant in a context of global change (Pörtner et al., 2022). The area of the present study lies within the transitional zone between the two biogeochemical regions defined by de Oliveira Carvalho et al. (2022). In this context, we focused the discussion on the possible physical and/or chemical-biological processes affecting the carbonate system distribution in the top 50 m along the COSTAL-AR section.

The likely strong CO_2 uptake and the fCO_2sw spatial variability found here over the different systems along the COSTAL-AR section in summer are in agreement with what was found previously at the Northern Argentine Continental Shelf (Bianchi et al., 2009; Kahl et al., 2017; Kahl, 2018; de Oliveira Carvalho et al., 2022). Nevertheless, some differences in the values of the carbonate system found between our results and previous observations may be due to the predominant processes occurring at the time of sampling.

Non-thermal effects, due to biological uptake and changes in mixing-stratification, evidently shaped the fCO_2sw spatial variability on the coastal and shelf systems in both summers; in addition, during VA-12/19 the presence of nutrient rich slope waters in the middle and outer shelf affected the fCO_2sw values (figures 2, 5, 6 and A2), as it has been found that upwelling also brings CO_2 (Hilligsøe et al., 2011). This is in accordance with Kahl et al. (2018) who suggested that the upwelling of deep waters at the edge of the slope, rich in DIC and nutrients, would transfer the carbon to the upper layer while the associated nutrient promotes the phytoplankton growth, which increases the biological CO_2 uptake. In our results the influence of the thermohaline gradient of the Shelf-break front in controlling the fCO_2sw distribution was evident in both cruises.

Biological driven processes on continental shelves play a significant role in the variability of surface fCO_2sw and DIC (e.g. Borges et al., 2005; Chen et al., 2013; Takahashi et al., 2014, Gruber, 2015). Nevertheless, given the spatially heterogeneous distribution of the microbial communities it is complex to identify changes on fCO_2sw and DIC associated with

photosynthesis and respiration. Even more, although changes in the phytoplankton composition will exert an important control over CO_2 dynamics (Basu and Mackey, 2018; Takao et al., 2020) few attempts have been made in the Southwestern Atlantic Ocean to address this issue (e.g. Schloss et al., 2007; Carvalho et al., 2021; de Oliveira Carvalho et al., 2022). In this study we identified the importance of biological processes occurring during summer in an area in the Northern Argentine Continental Shelf. We found that during the VA-01/19 cruise fCO_2sw substantially decreased in the onshore side of the Shelf-break front when both Chla and DO exhibited their maxima, in association with the high biomass of *E. huxleyi* (figures 6, 9 and A3). High resolution underway Chla and fCO_2sw data allowed us to identify the carbon uptake by the phytoplankton and its potential to lower fCO_2sw on the shelf; but picophytoeukaryotes production occurring at the deep Chla maximum during summer could also have influenced surface fCO_2sw (Shadwick et al., 2011; Kitidis et al., 2012). It should also be taken into account that while Chla is a reasonable bulk proxy of total phytoplankton biomass, the biological impact on fCO_2sw may be in some cases masked by the use of Chla alone to represent phytoplanktonic biomass and productivity. During the VA-12/19 cruise, a minimum value of 216 µatm in fCO_2sw was found in the middle shelf region, coincident with a bloom of *Synechococcus sp.* This maximum in carbon biomass did not coincide with a maximum of Chla since cyanobacteria are known to usually have a high carbon-to-Chla ratio (e.g. Silva et al., 2009). A minimum DIC value (1963 µmol kg^{-1}) concomitant with a high pH (8.19) was also found; reinforcing the indication that *Synechococcus sp* was probably modulating the carbonate system due to the photosynthetic process in this location.

Although surface distribution of TA is normally controlled by the same physical processes that affect salinity (e.g. riverine input, precipitation and evaporation), the remineralization of organic matter may dominate in coastal and inner shelf regimes, affecting TA due to nutrient cycling (e.g. Wolf-Gladrow et al., 2007). Our results of the TA-salinity analysis did not point out to a particular source, rather a combination of coastal, shelf and offshore dynamic processes acting on the surface TA distribution along the COSTAL-AR section. During the VA-12/19 cruise it seemed evident the major salinity effect of slope waters affecting TA; while during the VA-01/19 cruise seawater dilution and evaporation effects did not have a strong influence on TA, even more, the TA-salinity relationship would be steep if we disregard the high salinity values (figures 7 and 8). In a

future, it would be interesting to include all possible sources influencing the TA variability (e.g. riverine-groundwater discharge and organic alkalinity; Kerr et al., 2021).

Changes in TA, DIC and pH consistent with organic matter remineralization were found during the VA-01/19 cruise, specifically near the bottom in the shallower coastal station where conspicuous high TA, DIC (figure 7) and nitrite concentration, and low values of pH and DO (figure 2) occurred in association with the presence of high bacterioplankton biomass (figure 9). Regarding the possible effect of calcification on TA, we cannot rule out that the coccolithophorid bloom occurring in the CT5 during VA-01/19 could have influenced the surface TA (e.g. Hutchins, 2011). Nevertheless, values of TA were within the expected range for this water mass, and microscope examination showed that *E. huxleyi* cells were apparently in healthy conditions (intact cells), indicating that probably at this stage of the bloom the photosynthesis overpassed the calcification effect in affecting the carbonate system.

Finally, the values and variations of the carbonate system buffer sensitivities (i.e. acid-base buffer factors ∂pH/∂TA, ∂pH/∂DIC and the Revelle factor) provide insight into the ocean's response to future CO_2 and pH levels and the regions that may be most sensitive to ocean acidification (e.g. Egleston et al., 2010; Takahashi et al., 2014; Hagens and Middelburg, 2016; Humphrey et al., 2018). The carbonate system buffer sensitivities found here are in accordance with general knowledge of today's ocean (Soetaert et al., 2007; Egleston et al., 2010; Jiang et al., 2019) and previous observations in the Northern Argentine Continental Shelf region (Orselli et al., 2018). Richier et al. (2018) demonstrated that phytoplankton community responses to changes in the carbonate system vary across different ocean basins according to the inherent buffer capacity. In agreement with these findings, the analysis of the carbonate system buffer sensitivities in association with the autotrophic communities, showed for the VA-01/19 cruise, that ∂pH/∂TA, ∂pH/∂DIC and the Revelle factor (Table A3) were significantly correlated with phytoplankton biomass (Spearman correlations; p-value<0.05; 0.71, -0.71 and 0.69, respectively). During the VA-12/19 cruise no significant correlations were found between carbonate system buffer sensitivities and phytoplankton biomass, though pH variations corresponded well to the phytoplankton biomass variability observed (0.89; p-value <0.05).

5. CONCLUDING REMARKS

The CO_2-induced warming and acidification anthropogenic stressors unequivocally affect the plankton communities (Pörtner et al., 2022), impacting the ecological services they provide. Most studies on the carbonate system in the marine environment are of large spatial scope, or based on models. The dynamics of the carbonate system in the continental shelves is extremely variable, and efforts to better understand their contribution to the global budget are being carried out worldwide. The Southwestern Atlantic Ocean, and the Argentine Continental Shelf in particular, still remain sparsely sampled in space and time. As atmospheric CO_2 concentration keeps on increasing, is relevant to follow the reaction of this productive and highly susceptible to ocean acidification region of the ocean (e.g. Orselli et al. 2018). Previous published carbonate system datasets from the Northern Argentine Continental Shelf were collected more than a decade ago, mainly during spring (October 2005-September 2006, Kahl et al., 2018; October 2008, Orselli et al., 2018), at a time when the annual globally average atmospheric CO_2 in the marine surface was about 10% lower than that of the present study (385.02 ppm for 2008 instead of 410.07 ppm for 2019; Dlugokencky and Tans, 2022, NOAA/Earth System Research Laboratory (ESRL),www.esrl.noaa.gov/gmd/ccgg/trends/).

Here new observations were used to analyze in a coupled way the physical, chemical and biological mechanisms affecting the carbonate system distributions in the Northern Argentine Continental Shelf region in two summer conditions. This area located in a transition, between previously defined biogeochemical regions, showed a high heterogeneity in the environmental variables, microbial communities, and therefore the carbonate system. Phytoplankton production, triggered by light - stratification and by the upwelling of nutrient rich slope waters, played a key role in modulating the carbonate system and the CO_2 uptake, as well as their spatial variability. The study region during the summer was likely an important CO_2 sink ($dfCO_2$ sea-air values of -87 ± 46 µatm during the VA-01/19 cruise and -112 ± 47 µatm during the VA-12/19 cruise), evidencing that organic carbon was being produced, and would be available for higher trophic levels, and/or export off the shelf. During summer the main contribution to CO_2 fixation was given by small cells, since the microbial community was dominated by picophytoplankton (<2 µm; e.g. *Synechococcus sp* and coccal picophytoeukaryotes). This small fraction is supposed to have a lower efficiency to uptake CO_2 than larger cells, and its abundance has been predicted to

increase due to global change (Behrenfeld et al., 2006). More observations like those presented here would be helpful to improve the effect of the different microbial fractions on the carbonate system.

In this global change context, the sum of local efforts to understand the role of continental shelves would contribute to achieve the United Nations Sustainable Development Goal 14-target 14.3 (https://sdgs.un.org/goals/goal14).

ACKNOWLEDGMENTS

This study, as part of the activities of the "Dinámica del Plancton Marino y Cambio Climático"(DiPlaMCC) program from Instituto Nacional de Investigación y Desarrollo Pesquero (INIDEP), was possible thanks to the collaboration of many colleagues, especially M. Veccia and A. Baldoni who participated in the preparation, data collection and physical oceanography data processing, P. Zorzoli who performed Winkler analysis during the VA-12/19 cruise, A. Martínez who collaborated in phytoplankton analysis during the VA-12/19 cruise, M. Luz Clara Tejedor and H. Fenco who calculated the Simpson Parameter, L. Allegra and A. Dogliotti for providing the satellite images, D. del Valle for helpful discussions, M. Bertelo and D. Acevedo who provided logistical and technical assistance and D. Maldonado for helping with figures design. We also like to thank the captains and crew of the *R/V Victor Angelescu* for the friendly welcome on board during the VA-01/19 and VA-12/19 cruises. We are grateful for the constructive comments provided by two anonymous reviewers who substantially improve the final manuscript. This study was supported by INIDEP and Comisión Técnica Mixta del Frente Marítimo (CTMFM). In addition, this study was partially financed by funds from CONICET-Inter-American Institute for Global Change Research (IAI-CRN3094), and GOA-ON-TOF (Pier-2-Peer 2018-2019) granted to C.F. Berghoff, V. A. Lutz and D. Pierrot. This research was carried out in part under the auspices of the Cooperative Institute for Marine and Atmospheric Studies (CIMAS), a Cooperative Institute of the University of Miami and the National Oceanic and Atmospheric Administration, cooperative agreement # NA20OAR4320472. This work contributes to LAOCA network initiative.

AUTHOR CONTRIBUTIONS

V.A.L. and R.M.N. designed and led the COSTAL research cruises. C.F.B. conceived the research questions of this study, led the data compilation, performed the analysis and interpretation of results, prepared the data visualization and wrote the manuscript. C.F.B, L.E., R.I.S., V.S., R.M.N., M.C.H., M.C. and V.A.L. collected and processed the chemical-biological data. D.P. contributed to the analysis of CO_2 fugacities data. L.E. contributed to the statistical analysis. D.P., L.E. and L.B. contributed to carbonate chemistry interpretation. R.I.S., V.S., R.M.N. and V.A.L. contributed with the biological interpretation. C.F.B, D.P. and V.A.L. played significant roles in securing funding for this effort. All authors discussed the results, read and approved the submitted version of the manuscript.

DATA AVAILABILITY STATEMENT

In situ observations of CO_2 fugacities during VA-01/19 cruise can be found on version 2021 of the Surface Ocean Carbon Atlas (SOCAT) database (Bakker et al., 2016, 2021) at https://www.socat.info/index.php/version-2021/. Expocode: 08D820190124.

Quality checked physical oceanographic data (CTD and TSG) are stored in Base Regional de Datos Oceanográficos database from Instituto Nacional de Investigación y Desarrollo Pesquero (BaRDO-INIDEP; Baldoni et al., 2008) and can be obtained upon request at https://www.inidep.edu.ar/datos-oceanograficos.

REFERENCES

Antacli, J.C., et al. 2018. Phytoplankton and protozooplankton on the southern Patagonian shelf (Argentina, 47˚-55˚ S) in late summer: Potentially toxic species and community assemblage structure linked to environmental features. J. Sea Res., 140, 63–80. https://doi.org/10.1016/j.seares.2018.07.012

Aoyama, M., et al., 2013. 2012 Inter-laboratory Comparison Study of a Reference Material for Nutrients in Seawater. Technical Report of the Meteorological Research Institute of Japan. https://doi.org/10.11483/mritechrepo.60

Arruda, R., et al., 2015. Air-sea CO_2 fluxes and the controls on ocean surface pCO_2 seasonal variability in the coastal and open-ocean southwestern Atlantic Ocean: a modeling study. Biogeosciences, 12(19), 5793-5809. https://doi.org/10.5194/bg-12-5793-2015

Astor, Y.M., Scranton, M.I., Muller-Karger, F., Bohrer, R., García, J., 2005. fCO_2 variability at the CARIACO tropical upwelling time series station. Mar. Chem. 97, 245-261. https://doi.org/10.1016/j.marchem.2005.04.001

Auad, G., Martos, P., 2012. Climate variability of the northern Argentinean shelf circulation: impact on *Engraulis anchoita*. Int. J. Ocean Clim. Syst. 3, 17-43. https://doi.org/10.1260/1759-3131.3.1.17

Bakker, D.C., et al., 2016. A multi-decade record of high-quality fCO_2 data in version 3 of the Surface Ocean CO_2 Atlas (SOCAT). Earth Syst. Sci. Data. 8, 383-413. https://doi.org/10.5194/essd-8-383-2016

Bakker, D. C., et al. 2021. Surface Ocean CO_2 Atlas Database Version 2021 (SOCATv2021). (NCEI Accession 0210711). NOAA National Centers for Environmental Information. Dataset. https://doi.org/10.25921/YG69-JD96. Last Access 06/01/2021.

Balch, W.M., et al., 2014. Surface biological, chemical, and optical properties of the Patagonian Shelf coccolithophore bloom, the brightest waters of the Great Calcite Belt. Limnol. Oceanogr. 59(5), 1715-1732. https://doi.org/10.4319/lo.2014.59.5.1715

Baldoni, A., 2021. BaRDO: corrección de salinidad de los datos CTD en las campañas 2019. INIDEP Res. Rep. 56, 1-48.

Baldoni, A., Molinari, G., Guerrero, R., Kruk, M., 2008. Base regional de datos oceanográficos (BaRDO) INIDEP. INIDEP Res. Rep. 13, 1-25.

Basu, S., Mackey, K.R., 2018. Phytoplankton as key mediators of the biological carbon pump: Their responses to a changing climate. Sustainability 10(3), 869. https://doi.org/10.3390/su10030869

Bates, N.R., et al., 2014. A time-series view of changing ocean chemistry due to ocean uptake of anthropogenic CO_2 and ocean acidification. Oceanography. 27, 126-141. https://www.jstor.org/stable/24862128

Bauer, J.E., Cai, W.J., Raymond, P.A., Bianchi, T.S., Hopkinson, C.S., Regnier, P.A., 2013. The changing carbon cycle of the coastal ocean. Nature 504(7478), 61-70. https://doi.org/10.1038/nature12857

Becker, S., et al., 2019. GO-SHIP Repeat Hydrography Nutrient Manual: The precise and accurate determination of dissolved inorganic nutrients in seawater, using Continuous

Flow Analysis methods. In: GO-SHIP Repeat Hydrography Manual: A Collection of Expert Reports and Guidelines. pp. 56. http://dx.doi.org/10.25607/OBP-555

Behrenfeld, M.J., et al., 2006. Climate-driven trends in contemporary ocean productivity. Nature 444, 752-755. https://doi.org/10.1038/nature05317

Bianchi, A.A., Massonneau, M., Olivera, R.M., 1982. Análisis estadístico de las características T-S del Sector Austral de la plataforma continental Argentina. Acta Oceanog. Arg. 3, 93-118.

Bianchi, A.A., et al., 2005. Vertical stratification and air-sea CO_2 fluxes in the Patagonian shelf. J. Geophys. Res. Oceans. 110, C7. https://doi.org/10.1029/2004JC002488

Bianchi, A.A., et al., 2009. Annual balance and seasonal variability of sea-air CO_2 fluxes in the Patagonia Sea: Their relationship with fronts and chlorophyll distribution. J. Geophys. Res. Oceans., 114, C3. https://doi.org/10.1029/2008JC004854

Bittig, H., et al., 2018. SCOR WG 142: Quality Control Procedures for Oxygen and Other Biogeochemical Sensors on Floats and Gliders. Recommendations on the conversion between oxygen quantities for Bio-Argo floats and other autonomous sensor platforms. https://doi.org/10.13155/45915

Booth, B., 1993. Estimating cell concentration and biomass of autotrophic plankton using microscopy. In: Kemp, P., Sherr, B., Sherr, E., Cole, J. (Eds.), Handbook of Methodology in Aquatic Microbial Ecology. Lewis Publishers, Boca Raton, FL, pp. 199-205.

Borges, A.V., Delille, B., Frankignoulle, M., 2005. Budgeting sinks and sources of CO_2 in the coastal ocean: Diversity of ecosystems counts. Geophys. Res. Lett. 32, L14601. https://doi.org/10.1029/2005GL023053

Braga, E.S., et al., 2008. Nutrient distributions over the Southwestern South Atlantic continental shelf from Mar del Plata (Argentina) to Itajaí (Brazil): Winter-summer aspects. Cont. Shelf Res. 28(13), 1649-1661. https://doi.org/10.1016/j.csr.2007.06.018

Bratbak, G., 1985. Bacterial biovolume and biomass estimations. Appl. Environ. Microbiol. 49(6), 1488-1493. https://doi.org/10.1128/aem.49.6.1488-1493.1985

Breland II, J.A., Byrne, R.H., 1993. Spectrophotometric procedures for determination of sea water alkalinity using bromocresol green. Deep Sea Res. Part I Oceanogr. Res. Pap. 40(3), 629-641. https://doi.org/10.1016/0967-0637(93)90149-W

Brown, C. W., Yoder, J. A., 1994. Coccolithophorid blooms in the global ocean. J. Geophys. Res. Oceans, 99(C4), 7467-7482. https://doi.org/10.1029/93JC02156

Cao, Z., Yang, W., Zhao, Y., Guo, X., Yin, Z., Du, C., Zhao, H., Dai, M. (2020). Diagnosis of CO_2 dynamics and fluxes in global coastal oceans. Natl. Sci. Rev. 7(4), 786-797. https://doi.org/10.1093/nsr/nwz105

Carreto, J., Lutz, V.A., Carignan, M.O., Colleoni, A.D.C., De Marco, S.G., 1995. Hydrography and chlorophyll a in a transect from the coast to the shelf-break in the Argentinian Sea. Cont. Shelf Res. 15(2-3), 315-336. https://doi.org/10.1016/0278-4343(94)E0001-3

Carvalho, F., Kohut, J., Oliver, M.J., Schofield, O., 2017. Defining the ecologically relevant mixed-layer depth for Antarctica's coastal seas. Geophys. Res. Lett. 44, 338–345. https://doi.org/10.1002/2016GL071205

Carvalho, A.C.O., Kerr, R., Mendes, C.R.B., Azevedo, J.L.L., Tavano, V. M., 2021. Phytoplankton strengthen CO_2 uptake in the South Atlantic Ocean. Prog. Oceanogr 190, 102476. https://doi.org/10.1016/j.pocean.2020.102476

Cepeda, G.D., et al., 2020. The impact of Río de la Plata plume favors the small-sized copepods during summer. Estuar. Coast. Shelf Sci. 245, 107000. https://doi.org/10.1016/j.ecss.2020.107000

Charrad M., Ghazzali N., Boiteau V., Niknafs A., 2014. NbClust: An R Package for Determining the Relevant Number of Clusters in a Data Set. J. Stat. Softw. 61(6): 1-36. https://doi.org/10.18637/jss.v061.i06

Chau, T. T. T., Gehlen, M., Chevallier, F. 2022. A seamless ensemble-based reconstruction of surface ocean pCO_2 and air-sea CO_2 fluxes over the global coastal and open oceans. Biogeosciences. 19, 1087-1109. https://doi.org/10.5194/bg-19-1087-2022

Chen, C.T.A., Borges, A.V., 2009. Reconciling opposing views on carbon cycling in the coastal ocean: Continental shelves as sinks and near-shore ecosystems as sources of atmospheric CO_2. Deep Sea Res. Part II: Top. Stud. Oceanogr. 56(8-10),578-590. https://doi.org/10.1016/j.dsr2.2009.01.001

Chen, C.T.A., Huang, T.H., Chen, Y.C., Bai, Y., He, X., Kang, Y., 2013. Air–sea exchanges of CO_2 in the world's coastal seas. Biogeosciences. 10, 6509-6544. https://doi.org/10.5194/bg-10-6509-2013

Chisholm, S.W., 1992. Phytoplankton Size. In: Falkowski P.G., Woodhead A.D., Vivirito K. (Eds.) Primary Productivity and Biogeochemical Cycles in the Sea. Environmental Science Research, vol. 43. Springer, Boston, MA.

Clayton, T.D., Byrne, R.H., 1993. Spectrophotometric seawater pH measurements: total hydrogen ion concentration scale calibration of m-cresol purple and at-sea results, Deep Sea Res. Part I Oceanogr. Res. Pap. 40, 2115-2129. https://doi.org/10.1016/0967-0637(93)90048-8

Cullen, J.J., 2015. Subsurface Chlorophyll Maximum Layers: Enduring Enigma or Mystery Solved?. Annu. Rev. Mar. Sci. 7, 207-239. https://doi.org/10.1146/annurev-marine-010213-135111

de Carvalho-Borges, M., Orselli, I.B., de Carvalho Ferreira, M.L., Kerr, R., 2018. Seawater acidification and anthropogenic carbon distribution on the continental shelf and slope of the western South Atlantic Ocean. J. Mar. Sys. 187, 62-81. https://doi.org/10.1016/j.jmarsys.2018.06.008

de Oliveira Carvalho, A.D.C., Kerr, R., Tavano, V.M., Mendes, C.R.B. 2022. The southwestern South Atlantic continental shelf biogeochemical divide. Biogeochemistry. 159(2), 139-158. https://doi.org/10.1007/s10533-022-00918-8

Derisio, C., Berghoff, C.F. Molinari, G., Negri R., Silva, R., 2018. Distribución y abundancia de la comunidad zooplanctónica en primavera (2016) y su relación con el ambiente en el área de distribución de prerreclutas de merluza (*Merluccius hubbsi*) del efectivo norte. Revista Frente Marítimo 25, 89-104.

Dickson, A. G. 1990. Standard potential of the reaction: AgCl(s) + 12H_2(g) = Ag(s) + HCl(aq), and the standard acidity constant of the ion HSO4$^-$ in synthetic sea water from 273.15 to 318.15 K. J. Chem. Thermodyn. 22, 113-127. https://doi:10.1016/0021-9614(90)90074-Z

Dickson, A.G., Goyet, C., 1994. Handbook of methods for the analysis of the various parameters of the carbon dioxide system in sea water. Version 2 (No. ORNL/CDIAC-74). Oak Ridge National Lab., Tennessee (United States). https://doi.org/10.2172/10107773

Dickson, A.G., Sabine, C.L., Christian, J.R. (Eds.) 2007. Guide to best practices for ocean CO_2 measurements. Sidney, British Columbia, North Pacific Marine Science Organization,

191pp. (PICES Special Publication 3; IOCCP Report 8). https://doi.org/10.25607/OBP-1342

Dlugokencky, E., Tans, P., 2022. Trends in atmospheric carbon dioxide, National Oceanic and Atmospheric Administration, Earth System Research Laboratory (NOAA/ESRL), http://www.esrl.noaa.gov/gmd/ccgg/trends/global.html, last access: 17 July 2021.

Dogliotti, A.I., Lutz, V.A., Segura, V., 2014. Estimation of primary production in the southern Argentine continental shelf and shelf-break regions using field and remote sensing data. Remote Sens. Environ. 140, 497-508. https://doi.org/10.1016/j.rse.2013.09.021

Doney, S., Fabry, V., Feely, R.A., Kleypas, J., 2009. Ocean acidification: the other CO_2 problem. Annu. Rev. Mar. Sci. 1, 169-192. https://doi.org/10.1146/annurev.marine.010908.163834

Edler, L., M. Elbrächter., 2010. The Utermöhl method for quantitative phytoplankton analysis. In: Karlson, B., Cusack, C., Bresnan, E. (Eds.). Microscopic and molecular methods for quantitative phytoplankton analysis. Intergovernmental Oceanographic Commission of UNESCO. IOC Manuals and Guides. Paris. pp. 110.

Egleston, E.S., Sabine, C.L., Morel F.M.M., 2010. Revelle revisited: buffer factors that quantify the response of ocean chemistry to changes in DIC and alkalinity. Glob. Biogeochem. Cycles. 24, GB1002. https://doi.org/10.1029/2008GB003407

Fontela, M., Velo, A., Gilcoto, M., Pérez, F.F., 2021. Anthropogenic CO_2 and ocean acidification in Argentine Basin Water Masses over almost five decades of observations. Sci. Total Environ. 779, 146570. https://doi.org/10.1016/j.scitotenv.2021.146570

Frankignoulle, M., 1994. A complete set of buffer factors for acid/base CO_2 system in seawater. J. Mar. Sys. 5, 111–118. https://doi.org/10.1016/0924-7963(94)90026-4

Friedlingstein, P., et al., 2022. Global Carbon Budget 2021. Earth Syst. Sci. Data 14, 1917-2005. https://doi.org/10.5194/essd-14-1917-2022

Garcia, H.E., et al., 2013. World Ocean Atlas 2013: Dissolved Oxygen, Apparent Oxygen Utilization, and Oxygen Saturation. Levitus, S., Mishonov, A. (Eds). NOAA Atlas NESDIS 75, 27 pp. http://doi.org/10.7289/V5J67DWD

Garcia, V.M., et al., 2008. Environmental factors controlling the phytoplankton blooms at the Patagonia shelf-break in spring. Deep Sea Res. Part I Oceanogr. Res. Pap. 55, 1150-1166. https://doi.org/10.1016/j.dsr.2008.04.011

Gattuso, J.P., et al., 2015. Contrasting futures for ocean and society from different anthropogenic CO_2 emissions scenarios. Science. 349, 6243. https://doi.org/10.1126/science.aac4722

Gattuso, J.P., Epitalon, J.M., Lavigne, H., Orr, J., 2020. seacarb: Seawater Carbonate Chemistry. R package version 3.2.13. https://CRAN.R-project.org/package=seacarb

Gonçalves-Araujo, R., De Souza, M.S., Mendes, C.R.B., Tavano, V.M., Pollery, R.C., Garcia, C.A.E., 2012. Brazil-Malvinas confluence: effects of environmental variability on phytoplankton community structure. J. Plankton Res. 34, 399-415. https://doi.org/10.1093/plankt/fbs013

Gruber, N., 2015. Ocean biogeochemistry: carbon at the coastal interface. Nature. 517, 148-149. https://doi.org/10.1038/nature14082

Guerrero, R.A., Piola, A.R., 1997. Masas de agua en la plataforma continental. El Mar Argentino y sus Recursos Pesqueros. 1, 107-118.

Guerrero, R.A., et al., 2014. The salinity signature of the cross-shelf exchanges in the Southwestern Atlantic Ocean: Satellite observations. J. Geophys. Res. Oceans. 119, 7794-7810. https://doi.org/10.1002/2014JC010113

Guinder, V.A., Malits, A., Ferronato, C., Krock, B., Garzón-Cardona, J., Martínez, A. 2020. Microbial plankton configuration in the epipelagic realm from the Beagle Channel to the Burdwood Bank, a Marine Protected Area in Sub-Antarctic waters. PLoS ONE 15, e0233156. https://doi.org/ 10.1371/journal.pone.0233156

Hagens, M., Middelburg, J.J., 2016. Generalised expressions for the response of pH to changes in ocean chemistry. Geochim. Cosmochim. Acta. 187, 334-349. https://doi.org/10.1016/j.gca.2016.04.012

Hillebrand, H., Dürselen, C.D., Kirschtel, D., Pollingher, U., Zohary, T., 1999. Biovolume calculation for pelagic and benthic microalgae. J Phycol. 35, 403-424. https://doi.org/10.1046/j.1529-8817.1999.3520403.x

Hilligsøe, K. M., Richardson, K., Bendtsen, J., Sørensen, L. L., Nielsen, T. G., Lyngsgaard, M. M. 2011. Linking phytoplankton community size composition with temperature,

plankton food web structure and sea–air CO_2 flux. Deep Sea Res. I 58(8), 826-838. https://doi.org/10.1016/j.dsr.2011.06.004

Holm-Hansen, O., Lorenzen, C.J., Holmes, R.W., Strickland, J.D., 1965. Fluorometric determination of chlorophyll. ICES J. Mar. Sci. 30, 3-15. https://doi.org/10.1093/icesjms/30.1.3

Humphreys, M.P., Daniels, C.J., Wolf-Gladrow, D. A., Tyrrell, T., Achterberg, E.P., 2018. On the influence of marine biogeochemical processes over CO_2 exchange between the atmosphere and ocean. Mar. Chem. 199, 1-11. https://doi.org/10.1016/j.marchem.2017.12.006

Hutchins, D., 2011. Forecasting the rain ratio. Nature. 476, 41–42. https://doi.org/10.1038/476041a

Iida, Y., Takatani, Y., Kojima, A., Ishii, M., 2021. Global trends of ocean CO_2 sink and ocean acidification: an observation-based reconstruction of surface ocean inorganic carbon variables. J. Oceanogr. 77, 323-358. https://doi.org/10.1007/s10872-020-00571- 5

Ito, R.G., Schneider, B., Thomas, H., 2005. Distribution of surface fCO_2 and air–sea fluxes in the Southwestern subtropical Atlantic and adjacent continental shelf. J. Mar. Syst. 56, 227-242. https://doi.org/10.1016/j.jmarsys.2005.02.005

Ito, R.G., Garcia, C.A.E., Tavano, V.M., 2016. Net sea-air CO_2 fluxes and modelled pCO_2 in the southwestern subtropical Atlantic continental shelf during spring 2010 and summer 2011. Cont. Shelf Res. 119, 68-84. https://doi.org/10.1016/j.csr.2016.03.013

Jiang, L.Q., Carter, B.R., Feely, R.A., Lauvset, S.K., Olsen, A., 2019. Surface ocean pH and buffer capacity: past, present and future. Sci. Rep. 9, 1-11. https://doi.org/10.1038/s41598-019-55039-4

Jones, J.G., 1979. A guide to methods for estimating microbial numbers and biomass in freshwaters. Freshwater Biological Association, London.

Kahl, L.C., Bianchi, A.A., Osiroff, A.P., Pino, D.R., Piola, A.R., 2017. Distribution of sea-air CO_2 fluxes in the Patagonian Sea: seasonal, biological and thermal effects. Cont. Shelf Res. 143, 18-28. https://doi.org/10.1016/j.csr.2017.05.011

Kahl, L.C., 2018. Dinámica del CO_2 en el Océano Atlántico Sudoccidental. PhD Thesis. Universidad de Buenos Aires. Facultad de Ciencias Exactas y Naturales.

Kaiser, H.F., 1960. The application of electronic computers to factor analysis. Educ. Psychol. Meas. 20, 141-151. https://doi.org/10.1177/001316446002000116

Kerr, D.E., Brown, P.J., Grey, A., Kelleher, B.P., 2021. The influence of organic alkalinity on the carbonate system in coastal waters. Mar. Chem. 237, 104050. https://doi.org/10.1016/j.marchem.2021.104050

Kitidis, V., et al., 2012. Seasonal dynamics of the carbonate system in the Western English Channel. Cont. Shelf Res. 42, 30–40. https://doi.org/10.1016/j.csr.2012.04.012

Laruelle, G.G., Lauerwald, R., Pfeil, B., Regnier, P., 2014. Regionalized global budget of the CO_2 exchange at the air-water interface in continental shelf seas. Glob. Biogeochem. Cycles. 28, 1199-1214. https://doi.org/10.1002/2014GB004832

Laruelle, G.G., Landschützer, P., Gruber, N., Tison, J.L., Delille, B., Regnier, P., 2017. Global high-resolution monthly pCO_2 climatology for the coastal ocean derived from neural network interpolation, Biogeosciences 14, 4545–4561, ttps://doi.org/10.5194/bg-14-4545-2017.

Lauvset, S.K., Gruber, N., Landschützer, P., Olsen, A., Tjiputra, J., 2015. Trends and drivers in global surface ocean pH over the past 3 decades. Biogeosciences 12, 1285-1298. https://doi.org/10.5194/bg-12-1285-2015

Lencina-Avila, J.M., Ito, R.G., Garcia, C.A.E., Tavano, V.M., 2016. Sea-air carbon dioxide fluxes along 35 S in the South Atlantic Ocean. Deep Sea Res. Part I: Oceanogr. Res. Pap. 115, 175-187. https://doi.org/10.1016/j.dsr.2016.06.004

Li, W.K.W., 1998. Annual average abundance of heterotrophic bacteria and *Synechococcus* in surface ocean waters. Limnol. Oceanogr. 43, 1746–1753. https://doi.org/10.4319/lo.1998.43.7.1746

Liutti, C.C., Kerr, R., Monteiro, T., Orselli, I.B.M., Ito, R.G., Garcia, C.A.E., 2021. Sea surface CO_2 fugacity in the southwestern South Atlantic Ocean: an evaluation based on satellite-derived images. Mar. Chem. 236, 104020. https://doi.org/10.1016/j.marchem.2021.104020

Loferer-Krößbacher, M., Klima, J., Psenner, R., 1998. Determination of bacterial cell dry mass by transmission electron microscopy and densitometric image analysis. Appl. Environ. Microbiol. 64, 688-694. https://doi.org/10.1128/AEM.64.2.688-694.1998

Lucas, A.J., Guerrero, R.A., Mianzan, H.W., Acha, E.M., Lasta, C.A., 2005. Coastal oceanographic regimes of the northern Argentine continental shelf (34–43°S). Estuar. Coast. Shelf Sci. 65, 405-420. https://doi.org/10.1016/j.ecss.2005.06.015

Lueker, T.J., Dickson, A.G., Keeling, C.D., 2000. Ocean pCO_2 calculated from dissolved inorganic carbon, alkalinity, and equations for K1 and K2: validation based on laboratory measurements of CO_2 in gas and seawater at equilibrium. Mar. Chem. 70, 105-119. https://doi.org/10.1016/S0304-4203(00)00022-0

Lui, H K., Chen, C.T. A., 2017. Reconciliation of pH25 and pH*insitu* acidification rates of the surface oceans: A simple conversion using only in situ temperature. Limnol. Oceanogr. Methods. 15, 328-335. https://doi.org/10.1002/lom3.10170

Lusquiños, A., Valdéz, A.J. 1971. Aportes al conocimiento de las masas de agua del Atlántico Sudoccidental. Serv. Hidrog. Naval (Buenos Aires), H 659, pp. 48.

Lutz, V.A., Carreto, J.I., 1991. A new spectrofluorometric method for the determination of chlorophylls and degradation products and its application in two frontal areas of the Argentine Sea. Cont. Shelf Res., 11, 433-451. https://doi.org/10.1016/0278-4343(91)90052-8

Lutz, V.A., Segura, V., Dogliotti, A.I., Gagliardini, D.A., Bianchi, A.A., Balestrini, C.F., 2010. Primary production in the Argentine Sea during spring estimated by field and satellite models. J. Plankton Res. 32, 181-195. https://doi.org/10.1093/plankt/fbp117

Marañón, E., 2015. Cell size as a key determinant of phytoplankton metabolism and community structure. Annu. Rev. Mar. Sci. 7, 241-264. https://doi.org/10.1146/annurev-marine-010814-015955

Margalef, R. 1978. Life-forms of phytoplankton as survival alternatives in an unstable environment. Oceanologica Acta, 1, 493-509.

Marrari, M., et al., 2013. Reproductive success of the Argentine anchovy, *Engraulis anchoita*, in relation to environmental variability at a mid-shelf front (Southwestern Atlantic Ocean). Fish. Oceanogr. 22, 247-261. https://doi.org/10.1111/fog.12019

Marrari, M., Piola, A.R., Valla, D., 2017. Variability and 20-year trends in satellite-derived surface chlorophyll concentrations in large marine ecosystems around South and Western Central America. Front. Mar. Sci. 4, 372. https://doi.org/10.3389/fmars.2017.00372

Martos, P., Piccolo, M.C., 1988. Hydrography of the Argentine continental shelf between 38 and 42 ˚S. Cont. Shelf Res. 8, 1043-1056. https://doi.org/10.1016/0278-4343(88)90038-6

Matano, R. P., Palma, E. D., Piola, A. R., 2010. The influence of the Brazil and Malvinas Currents on the Southwestern Atlantic Shelf circulation. Ocean Sci. 6, 983-995. https://doi.org/10.5194/os-6-983-2010.

Menden-Deuer, S., Lessard, E.J., 2000. Carbon to volume relationships for dinoflagellates, diatoms, and other protist plankton. Limnol. Oceanogr. 45, 569-579. https://doi.org/10.4319/lo.2000.45.3.0569

Millero, F.J., Zhang, J.-Z., Lee, K., Campbell, D.M., 1993. Titration alkalinity of seawater. Mar. Chem. 44, 153–165. https://doi.org/10.1016/0304-4203(93)90200-8

Millero, F.J., Lee, K., Roche, M., 1998. Distribution of alkalinity in the surface waters of the major oceans. Mar. Chem. 60, 111-130. https://doi.org/10.1016/S0304-4203(97)00084-4

Möller, O.O., Piola, A.R., Freitas, A.C., Campos, E.J.D., 2008. The effects of river discharge and seasonal winds on the shelf off southeastern South America. Cont. Shelf Res. 28, 1607–1624. https://doi.org/10.1016/j.csr.2008.03.012

Negri, R.M. et al., 2016. Ambiente y Plancton en la Zona Común de Pesca Argentino-Uruguaya en un escenario de cambio climático (marzo, 2014). Frente Marítimo. 24, 251.

Orr, J.C. et al., 2005. Anthropogenic ocean acidification over the twenty-first century and its impact on calcifying organisms. Nature. 437, 681-686. https://doi.org/10.1038/nature04095

Orselli, I.B., Kerr, R., Ito, R.G., Tavano, V.M., Mendes, C.R.B., Garcia, C.A., 2018. How fast is the Patagonian shelf-break acidifying?. J. Mar. Syst. 178: 1-14. https://doi.org/10.1016/j.jmarsys.2017.10.007

Padin, X.A., et al., 2010. Air-Sea CO_2 fluxes in the Atlantic as measured during boreal spring and autumn. Biogeosciences. 7, 1587-1606. https://doi.org/10.5194/bg-7-1587-2010

Peres-Neto, P.R., Jackson, D.A., Somers, K.M., 2003. Giving meaningful interpretation to ordination axes: assessing loading significance in principal component analysis. Ecology. 84, 2347-2363. https://doi.org/10.1890/00-0634

Pierrot, D., et al., 2009. Recommendations for autonomous underway pCO_2 measuring systems and data-reduction routines. Deep Sea Res. Part II: Top. Stud. Oceanogr. 56(8-10): 512-522. https://doi.org/10.1016/j.dsr2.2008.12.005

Piola, A.R., Campos, E.J., Möller Jr, O.O., Charo, M., Martinez, C., 2000. Subtropical shelf front off eastern South America. J. Geophys. Res. Oceans. 105, 6565-6578. https://doi.org/10.1029/1999JC000300

Piola, A.R., Matano, R.P., 2001. Brazil and Falklands (Malvinas) currents. In: Steele, J.M., Thorpe, S.A., Turekian, K.K. (Eds.). Encyclopedia of Ocean Sciences, 2nd ed., Academic Press, London. pp. 340–349.

Piola, A.R., Martínez Avellaneda, N., Guerrero, R.A., Jardon, F.P., Palma, E.D., Romero, S.I., 2010. Malvinas-slope water intrusions on the northern Patagonia continental shelf. Ocean Sci. 6, 345-359. https://doi.org/10.5194/os-6-345-2010

Porter, K.G., Feig, Y.S., 1980. The use of DAPI for identifying and counting aquatic microflora. Limnol. Oceanogr. 25, 943-948. https://doi.org/10.4319/lo.1980.25.5.0943

Pörtner, H.O., et al., 2022. Climate Change 2022: Impacts, Adaptation, and Vulnerability. Contribution of Working Group II to the Sixth Assessment Report of the Intergovernmental Panel on Climate Change (IPCC). Cambridge University Press. In Press.

Posch, T., Loferer-Krößbacher, M., Gao, G., Alfreider, A., Pernthaler, J., Psenner, R., 2001. Precision of bacterioplankton biomass determination: a comparison of two fluorescent dyes, and of allometric and linear volume-to-carbon conversion factors. Aquat. Microb. Ecol. 25, 55-63. https://doi.org/10.3354/ame025055

Poulton, A. J. et al., 2013. The 2008 *Emiliania huxleyi* bloom along the Patagonian Shelf: Ecology, biogeochemistry, and cellular calcification. Global Biogeochem Cycles, 27(4), 1023-1033. doi: 10.1002/2013GB004641.

Putt, M., Stoecker, D.K. 1989. An experimentally determined carbon: volume ratio for marine “oligotrichous” ciliates from estuarine and coastal waters. Limnol. Oceanogr. 34, 1097-1103. https://doi.org/10.4319/lo.1989.34.6.1097

R Core Team, 2021. R: A language and environment for statistical computing. R Foundation for Statistical Computing, Vienna, Austria. (http://www.R-project.org/).

Raven, J.A. 1998. The twelfth Tansley Lecture. Small is beautiful: the picophytoplankton. Funct. Ecol. 12(4): 503–513.

Richier, S., et al., 2018. Geographical CO_2 sensitivity of phytoplankton correlates with ocean buffer capacity. Glob. Change Biol. 24, 4438-4452. https://doi.org/10.1111/gcb.14324

Riebesell, U., Körtzinger, A., Oschlies, A., 2009. Sensitivities of marine carbon fluxes to ocean change. Proc. Natl. Acad. Sci. 106, 20602-20609. https://doi.org/10.1073/pnas.0813291106

Roobaert, A., Laruelle, G.G., Landschützer, P., Gruber, N., Chou, L., Regnier, P., 2019. The spatiotemporal dynamics of the sources and sinks of CO_2 in the global coastal ocean. Glob. Biogeochem. Cycles 33(12), 1693-1714. https://doi.org/10.1029/2019GB006239

Romero, S.I., Piola, A.R., Charo, M., Garcia, C.A.E., 2006. Chlorophyll-a variability off Patagonia based on SeaWiFS data. J. Geophys. Res. 111, C05021. https://doi.org/10.1029/2005JC003244

Sánchez, R.P., Bezzi, S.I. (Eds.), 2004. El Mar Argentino y sus recursos pesqueros. Tomo 4. Los peces marinos de interés pesquero. Caracterización biológica y evaluación del estado de explotación. Publicaciones Especiales INIDEP, Mar del Plata. pp. 359

Saraceno, M., Provost, C., 2012. On eddy polarity distribution in the southwestern Atlantic. Deep Sea Res. Part I: Oceanogr. Res. Pap. 69, 62-69. https://doi.org/10.1016/j.dsr.2012.07.005

Schlitzer, R., 2021. Ocean Data View. (https://odv.awi.de).

Schloss, I.R., et al., 2007. Role of plankton communities in sea–air variations in pCO_2 in the SW Atlantic Ocean. Mar. Ecol. Prog. Ser. 332, 93-106. https://doi.org/10.3354/meps332093

Scott, A. J., Knott, M. 1974. A Cluster Analysis Method for Grouping Means in the Analysis of Variance. Biometrics. 30, 507–512. https://doi.org/10.2307/2529204

Segura, V. et al., 2013. Phytoplankton types and primary production in the Argentine Sea. Mar. Ecol. Prog. Ser. 491, 15-31. https://doi.org/10.3354/meps10461

Shadwick, E.H. et al., 2011. Seasonal variability of dissolved inorganic carbon and surface water pCO_2 in the Scotian Shelf region of the Northwestern Atlantic. Mar. Chem. 124, 23-37. https://doi.org/10.1016/j.marchem.2010.11.004

Sieburth, J.M., Smetacek, V., Lentz, J., 1978. Pelagic ecosystem structure: Heterotrophic compartments of the plankton and their relationship to plankton size fractions. Limnol. Oceanogr. 23, 1256-1263. https://doi.org/10.4319/lo.1978.23.6.1256

Signorini, S.R., Garcia, V.M.T., Piola, A.R., Garcia, C.A.E., Mata, M.M., McClain, C.R., 2006. Seasonal and interannual variability of calcite in the vicinity of the Patagonian shelf break (38°S–52°S). Geophys. Res. Lett. 33, L16610. https://doi.org/10.1029/2006GL026592

Silva, R.I., Negri, R.M., Lutz, V.A., 2009. Summer succession of ultraphytoplankton at the EPEA coastal station (Northern Argentina). J. Plankton Res. 31 (4): 447-458. https://doi.org/10.1093/plankt/fbn128

Soetaert, K., Hofmann, A.F., Middelburg, J.J., Meysman, F.J., Greenwood, J., 2007. Reprint of "The effect of biogeochemical processes on pH". Mar. Chem. 106, 380-401. https://doi.org/10.1016/j.marchem.2007.06.008

Strickland, J.D.H., Parsons, T.R., 1972. A practical handbook of seawater analysis. Fisheries Research Board of Canada, Otawa.

Sundquist, E.T., Plummer, L.N., Wigley, T.M.L., 1979. Carbon dioxide in the ocean surface: the homogeneous buffer factor. Science. 204, 1203-1205. https://doi.org/10.1126/science.204.4398.1203

Sverdrup, H.U., 1953. On conditions for the vernal blooming of phytoplankton. J. Conseil Exp. Mer. 187,287-295.

Takahashi, T., Olafsson, J., Goddard, J., Chipman, D.W., Sutherland, S.C., 1993. Seasonal variation of CO_2 and nutrients in the high-latitude surface oceans: a comparative study. Glob. Biogeochem. Cycles 7, 843-878. https://doi.org/10.1029/93GB02263

Takahashi, T., et al., 2002. Global sea-air CO_2 flux based on climatological surface ocean pCO_2, and seasonal biological and temperature effects. Deep Sea Res. Part II: Top. Stud. Oceanogr. 49, 1601-1622. https://doi.org/10.1016/S0967-0645(02)00003-6

Takahashi, T., et al., 2009. Climatological mean and decadal change in surface ocean pCO_2, and net sea–air CO_2 flux over the global oceans. Deep Sea Res. Part II: Top. Stud. Oceanogr. 56, 554-577. https://doi.org/10.1016/j.dsr2.2008.12.009

Takahashi, T., Sutherland, S. C., Chipman, D.W., Goddard, J.G., Ho, C., Newberger, T., Sweeney, C., Munro, D.R., 2014. Climatological distributions of pH, pCO_2, total CO_2, alkalinity, and $CaCO_3$ saturation in the global surface ocean, and temporal changes at selected locations. Mar. Chem. 164, 95-125. https://doi:10.1016/j.marchem.2014.06.004.

Takao, S., et al., 2020. Effects of phytoplankton community composition and productivity on sea surface pCO2 variations in the Southern Deep-Sea Res. I: Oceanogr. Res. Pap., 160, 103263. https://doi.org/10.1016/j.dsr.2020.103263

Temperoni, B., Luz Clara, M., Berghoff, C., Derisio, C., Massa, A.E., 2021. The effect of physical and biological variables upon condition of *Merluccius hubbsi* (age-0+) of the northern stock (Argentine Shelf, SW Atlantic Ocean). J. Mar. Sys. 224, 103620. https://doi.org/10.1016/j.jmarsys.2021.103620

Uppström L.R., 1974. The boron/chlorinity ratio of the deep-sea water from the Pacific Ocean. Deep Sea Res. Oceanogr. Abstracts, 21, 161-162. https://doi.org/10.1016/0011-7471(74)90074-6

Volk, T., Hoffert, M.I., 1985. Ocean carbon pumps: Analysis of relative strengths and efficiencies in ocean-driven atmospheric CO_2 changes. In: Sundquist, E., Broecker, W. (Eds.). The carbon cycle and atmospheric CO_2: natural variations Archean to present, 32: 99-110. https://doi.org/10.1029/GM032p0099

Weber Jr, W.J., Stumm, W. 1963. Mechanism of hydrogen ion buffering in natural waters. J. - Am. Water Works Assoc. 55, 1553-1578. https://doi.org/10.1002/j.1551-8833.1963.tb01178.x

Wolf-Gladrow, D.A., Zeebe, R.E., Klaas, C., Körtzinger, A., Dickson, A.G., 2007. Total alkalinity: The explicit conservative expression and its application to biogeochemical processes. Mar. Chem. 106, 287-300. https://doi.org/10.1016/j.marchem.2007.01.006

SUPPLEMENTARY MATERIAL

Table A1. Geographical position and total depth of stations along the COSTAL-AR section, as well as date-time of sampling during the VA-01/19 and VA-12/19 cruises.

Station	Latitude (°S)	Longitude (°W)	Depth (m)	VA-01/19	VA-12/19
				Date and Time (UTC)	Date and Time (UTC)
CT1	-38.22	-57.28	40	24/1/2019 19:20	12/12/2019 09:13
CT2	-38.35	-57.03	70	24/1/2019 22:44	13/12/2019 12:38
CT3	-38.48	-56.75	80	26/1/2019 21:35	13/12/2019 16:28
CT4	-38.74	-56.25	90	26/1/2019 16:44	11/12/2019 19:23
CT5	-39.08	-55.73	120	26/1/2019 10:03	11/12/2019 15:04
CT6	-39.38	-55.22	950	25/1/2019 22:44	11/12/2019 09:05

Table A2. List of acronyms and symbols used in the main text.

Acronyms and Symbols	Description	Units
∂pH/∂DIC	Acid-base buffer factor expressing the change in pH relative to a change in DIC	$(mol\ kg^{-1})^{-1}$
∂pH/∂TA	Acid-base buffer factor expressing the change in pH relative to a change in TA	$(mol\ kg^{-1})^{-1}$
BT_A	Ratio of the amplitudes of non-thermal over thermal effects	dimensionless
Chla	Chlorophyll a concentration	$mg\ m^{-3}$
$dfCO_2$ sea-air	Difference between fCO_2sw and fCO_2air	µatm
DIC	Dissolved inorganic carbon	$\mu mol\ kg^{-1}$
DO	Dissolved oxygen	$\mu mol\ kg^{-1}$
fCO_2air	Fugacity of CO_2 in air	µatm
fCO_2sw	Fugacity of CO_2 in seawater	µatm
Non-therm	Non-thermal effects on the changes of fCO_2sw	µatm
$Non\text{-}therm_A$	Amplitudes of non-thermal effects	µatm
NTA	Total alkalinity normalized to salinity of 35	$\mu mol\ kg^{-1}$
pCO_2	Partial pressure of CO_2	µatm
PTA	Potential total alkalinity	$\mu mol\ kg^{-1}$
TA	Total alkalinity	$\mu mol\ kg^{-1}$
Therm	Thermal effects on the changes of fCO_2sw	µatm
$Therm_A$	Amplitudes of thermal effects	µatm

Cluster analysis from vertical thermohaline, chlorophyll a, and dissolved oxygen properties

VA-01/19 cruise. An optimal number of five clusters (CLUS) were determined (figure A1, left). CLUS-1 gathered data from the surface mixed layer from all sampled stations (Temp 18.9 ± 1.4 ^{o}C); CLUS-5 comprised all stations but CT6 from depths below the mixed layer, and CLUS-4 gathered samples from the highest average salinity (35.15 ± 0.19), including only station CT6 below the mixed layer. On the other hand, CLUS-2 and CLUS-3 associated samples from the noticeable deep Chla and DO maxima found in the middle and outer shelf (stations CT3 to CT5).

VA-12/19 cruise. An optimal number of four CLUS were determined (figure A1, right). CLUS-1 and CLUS-3 gathered samples associated with shelf waters with salinity <33.7. CLUS-2 and CLUS-4 comprised data on the outer stations (CT5 and CT6) where slope waters signal was observed in the profile (salinity >34.1 and DO >300 µmol kg^{-1}). Both CLUS-1 and CLUS-2 were associated with high Chla values. CLUS-3 included data in the middle shelf below the thermocline (stations CT3 and CT4) associated with the lowest DO values (254 ± 13 µmol kg^{-1}).

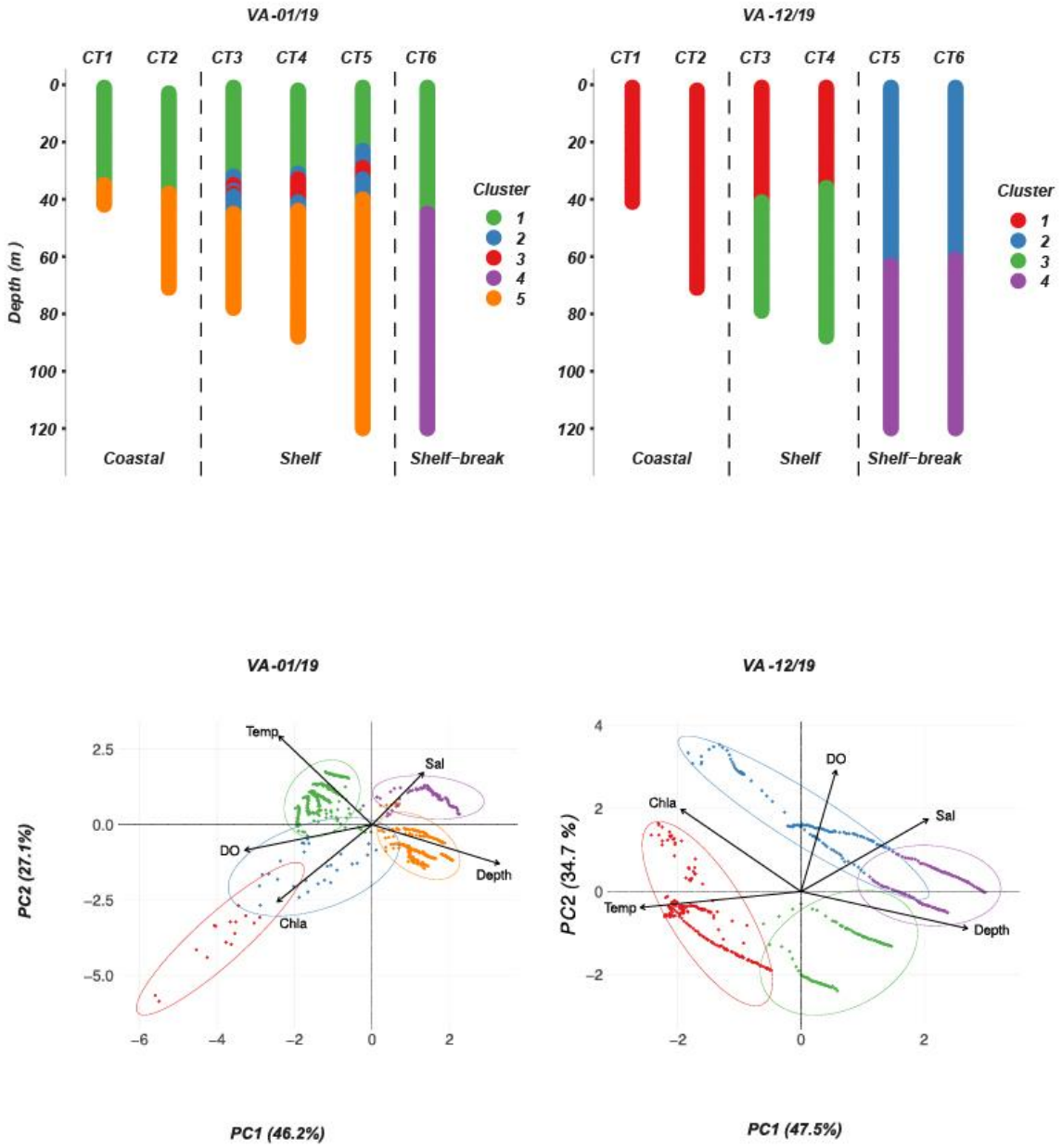

Figure A1. Top: Profiles of the sampling stations along the COSTAL-AR section, with colors representing the distribution of the clusters groups determined by the NbClust approach; dashed lines separate the main oceanographic systems established by gathering cluster's shared stations. Bottom. Principal component analysis biplot of temperature (Temp, °C), salinity (Sal), depth (m), dissolved oxygen (DO, µmol kg^{-1}) and chlorophyll a (Chla, mg m^{-3}) along the COSTAL-AR section during summer, showing the PC scores (dots) of profile observations. encircled in correspondence with the cluster groups determined by the NbClust approach. Left: VA-01/19 cruise; right: VA-12/19 cruise.

Processes influencing the DO and fCO_2sw distributions

More than one process is usually responsible for controlling CO_2 concentrations. Property-property relations of the percentage of saturation of fCO_2 (fCO_2sat) versus DO (DOsat) relative to the atmosphere were explored in an attempt to visualize the relative role of physical and chemical-biological processes influencing the DO and fCO_2sw distributions. fCO_2sat was calculated as the fCO_2sw/fCO_2air ratio. DOsat was estimated according to Garcia et al. (2013). The fCO_2sat versus DOsat distributions were analyzed by its position relative to the 100% saturation levels of DO and CO_2 (figure A3). Simultaneous fCO_2sw undersaturation and DO supersaturation occurs, implies the dominance of non-thermal processes, e.g., photosynthesis. This is the case observed on the shelf and shelf-break along the COSTAL-AR section, while the temperature effect seems to dominate both coastal fCO_2sw and DO saturation.

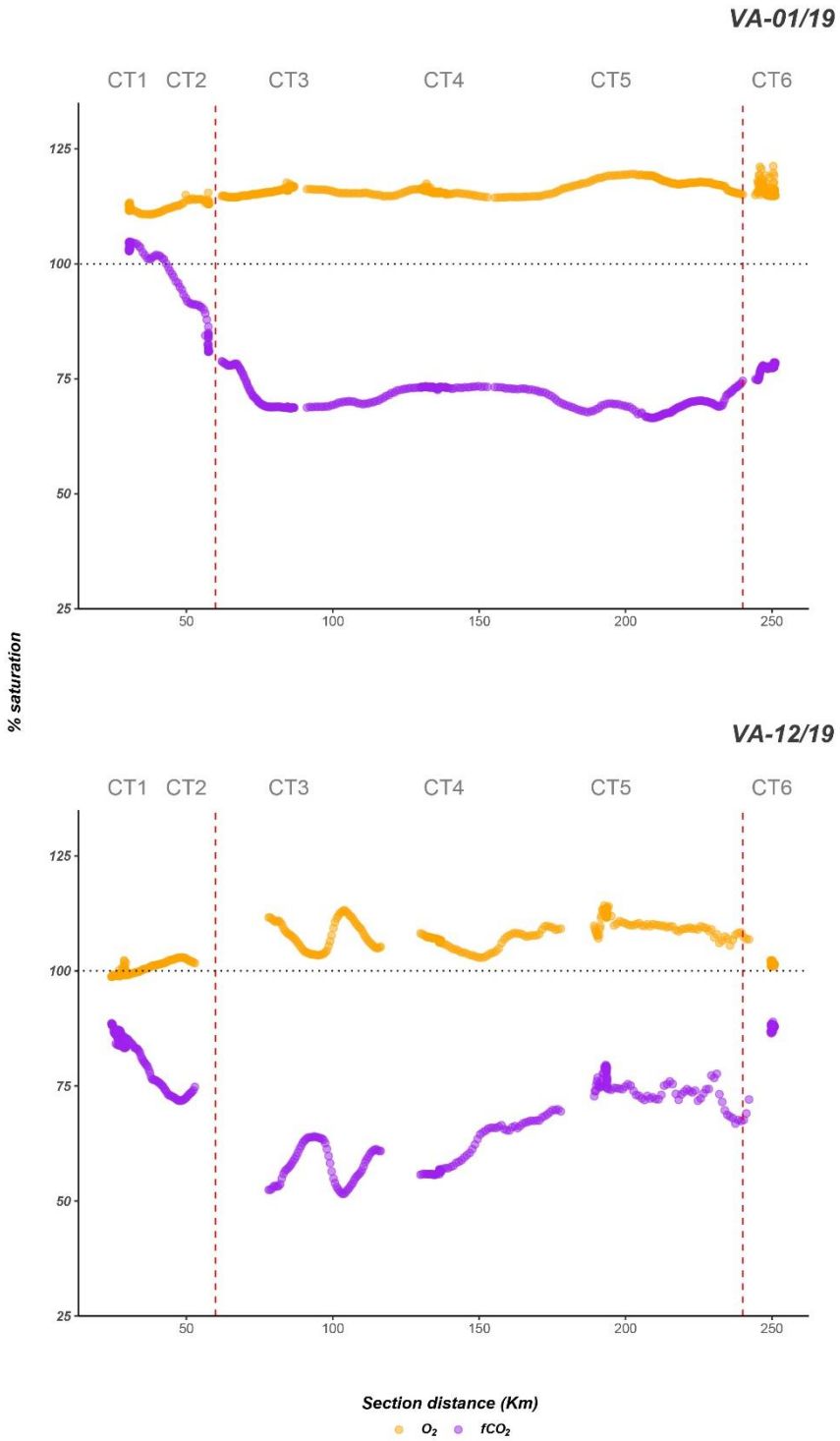

Figure A2. Property-property plot of percentage of saturation (y-axis) of fCO_2 (purple) and DO (orange) along the COSTAL-AR section distance (Km; x-axis). Top: VA-01/19 cruise; bottom: VA-12/19 cruise. Horizontal dotted line represent the 100% saturation levels of DO and CO_2. that helps infer the dominating processes controlling the fCO_2sw and DO distribution (see text for more details). The vertical dotted red lines separate the main oceanographic systems established by the change point method. Station positions are also indicated.

Table A3. Vertical properties data (mean ± SD) of pH, total alkalinity (TA, µmol kg^{-1}), dissolved inorganic carbon (DIC, µmol kg^{-1}) and dissolved inorganic nutrients (nitrate, nitrite, silicate and phosphate; µmol kg^{-1}) in the top 120 meters along the different systems in COSTAL-AR section that were established by the cluster analysis. Number of observations are indicated in parenthesis.

	VA-01/19									
	Station	*pH*	*TA*	*DIC*	*Nitrate*	*Nitrite*	*Silicate*	*Phosphate*	*∂pH/∂TA*	*∂pH/∂DIC*	*Revelle*
Coastal	CT1-CT2	8.00 ± 0.08 (6)	2289.3 ± 52 (6)	2080.5 ± 84 (6)	1.93 ± 3.7 (6)	0.25 ± 0.4 (6)	3.04 ± 2.7 (6)	0.74 ± 0.5 (6)	2027± 374 (6)	-2155± 351 (6)	12 ± 2 (6)
Shelf	CT3-CT5	7.988 ± 0.14 (12)	2238.1 ± 7 (10)	2063.8 ± 91 (10)	8.84 ± 7.2 (12)	0.07 ± 0.06 (12)	3.39 ± 2.4 (12)	0.94 ± 0.6 (12)	2381± 662 (10)	-2491 ± 617 (10)	13.5 ± 3 (10)
Shelf-Break	CT6	8.078 ± 0.03 (4)	2300.8 ± 21 (3)	2052.3 ± 54 (3)	2.48 ± 2.4 (4)	0.06 ± 0.07 (4)	1.96 ± 0.9 (4)	0.33 ± 0.2 (4)	1783± 159 (3)	-1925 ± 148 (3)	10.8 ± 1 (3)

	VA-12/19									
	Station	*pH*	*TA*	*DIC*	*Nitrate*	*Nitrite*	*Silicate*	*Phosphate*	*∂pH/∂TA*	*∂pH/∂DIC*	*Revelle*
Coastal	CT1-CT2	8.073 ± 0.02 (7)	2262.9 ± 7 (4)	2040.1 ± 20 (4)	0.27 ± 0.2 (7)	0.03 ± 0.03 (7)	1.15 ± 0.8 (7)	0.67 ± 0.1 (7)	19267 ± 86 (4)	-2064 ± 80 (4)	11.4 ± 1 (4)
Shelf	CT3-CT4	8.078 ± 0.13 (8)	2257.5 ± 7 (4)	2062.8 ± 94 (4)	2.43 ± 3 (8)	0.07 ± 0.09 (8)	2.6 ± 1.7 (8)	0.88 ± 0.7 (8)	2247 ± 679 (4)	-2365 ± 637 (4)	13 ± 3 (4)
Shelf-Break	CT5-CT6	8.062 ± 0.03 (8)	2277.2 ± 16 (4)	2101.3 ± 35 (4)	6.18 ± 1.2 (7)	0.18 ± 0.05 (7)	2.9 ± 1.3 (7)	1.2 ± 0.3 (7)	2254 ± 240 (4)	-2371 ± 226 (4)	13.1 ± 1 (4)

Table A4. TA-salinity and TA-DIC least square regression equations, correlation coefficients (r^2) and RMSE obtained in the top 50 m for the VA-01/19 and VA-12/19 cruise. n: number of observations used to develop these correlations.

TA-Salinity	Equation	r^2	RMSE	n
VA-01/19	TA= 52 Sal + 515	0.27	38.7	14
VA-01/19 (excluding sample from bottom at station CT1)	TA= 54.7 Sal + 413	0.66	18.5	13
VA-12/19	TA= 33.2 Sal + 1143.6	0.76	5.2	7

TA-DIC	Equation	r^2	RMSE	n
VA-01/19	TA= 0.5 DIC + 1259.6	0.73	23.6	14
VA-01/19 (excluding sample from bottom at station CT1)	TA= 0.4 DIC + 1474.4	0.47	23.3	13
VA-12/19	TA= 0.1 DIC + 2011.9	0.29	8.8	7

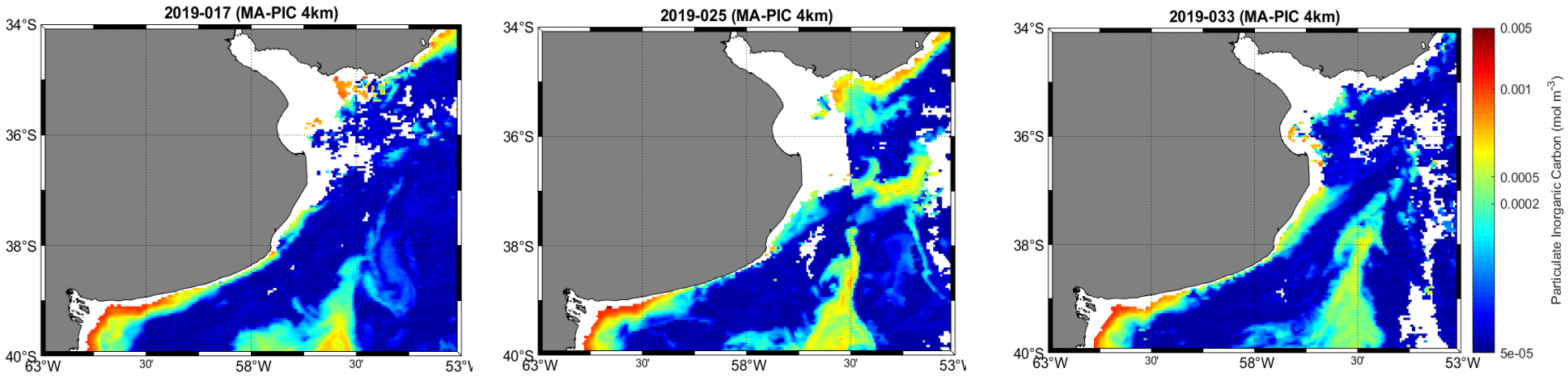

Figure A3. MODIS-Aqua 8-day Particulate Inorganic Carbon (PIC) concentration (mol m^{-3}) composite image (4 km resolution) in the Northern Argentinean Continental Shelf for the period of the VA-01/19 cruise. Left: 17-24 January 2019; center: 25 January 2019- 1 February 2019; right: 2-9 February 2019.